Isospin dependent global nucleon-nucleus optical model at intermediate energies

S. P. Weppner,[*] R. B. Penney,[†] G. W. Diffendale,[‡] and G. Vittorini[§]
Natural Sciences, Eckerd College, St. Petersburg, Florida 33711, USA
(Received 19 December 2008; revised manuscript received 18 June 2009; published 15 September 2009)

A global nucleon-nucleus optical potential for elastic scattering has been produced which replicates experimental data to high accuracy and compares well with other recently formulated potentials. The calculation that has been developed describes proton and neutron scattering from target nuclei ranging from carbon to nickel and is applicable for projectile energies from 30 to 160 MeV. With these ranges it is suitable for calculations associated with experiments performed by exotic beam accelerators. The potential has both real and imaginary isovector asymmetry terms to better describe the dynamics of chains of isotopes and mirror nuclei. An analysis of the validity and strength of the asymmetry term is included with connections established to other optical potentials and charge-exchange reaction data.

DOI: 10.1103/PhysRevC.80.034608 PACS number(s): 24.10.Ht, 21.30.Fe, 25.40.Cm, 25.40.Dn

I. INTRODUCTION

The fitting of global nucleon-nucleus optical model potentials (OMP) for elastic scattering has a venerable history [1–10]. The global optical potential of this work (WP OMP) was specifically designed with the next generation of radioactive beam accelerators in mind. It attempts to fit a lighter range of targets ($12 \leqslant A \leqslant 60$), including those far from stability, and it is over a limited projectile energy range ($30\ \text{MeV} \leqslant E \leqslant 160\ \text{MeV}$). This research has produced one continuous global isospin dependent OMP which incorporates both proton and neutron scattering and real and imaginary isovector asymmetry terms. Overall the potential of this work is recommended if one is interested in examining trends in the light and medium nuclei, specifically isospin asymmetry dependencies, shell closure, and neutron excess in isotopes. Since the elastic potential is often used as a starting point in developing further inelastic results, this global optical potential will give the researcher a consistent formulation over a wide variety of nuclei from which to generate multichannel calculations. To promote its use we provide an on-line optical potential calculator [11].

Recently there has been the development of two other modern global OMPs for nucleon-nucleus elastic scattering which cover an extensive projectile energy and target range: the potentials of Koning and Delaroche (KD OMP) [1] and Madland (MD OMP) [2]. Specifically the potential of Ref. [1] has set an impressive benchmark for its extensive projectile energy range (1 keV to 200 MeV) and its accuracy of fit. We will make theoretical and calculatable comparisons of the new WP OMP to these noteworthy potentials throughout this article.

In Sec. II we briefly discuss the theory of the global optical potential. A summary of our theoretical fitting procedure and the experimental reactions constraining the fit follows in Sec. III. A generous amount of example calculations, given in Sec. IV, compare the results of this potential with the two other contemporary optical potentials. This is followed, in Sec. V, by a detailed analysis of the isovector asymmetric term identifying dramatic differences in the magnitude and character of the isovector asymmetry $N - Z$ term of the three global OMPs as well as with standard $t - \rho$ microscopic potentials. Reactions are isolated which would better constrain the isovector term in the future. We end with concluding remarks and future directions.

II. THEORY

The theoretical and computational aspects of creating a global optical potential have been discussed in detail elsewhere, we only mention a few works which were found to be especially useful for this research. The seminal work of Melkanoff *et al.* [12] discusses in thorough detail many of the hurdles that need to be overcome when attempting a computational fitting of nuclear scattering data. Beccetti and Greenless [3] created the first comprehensive and still viable global optical potential, we especially found poignant their discussion on weighting the various observables. Recently Koning and Delaroche have provide the nuclear physics community with an ambitious optical model potential (KD OMP) [1] as previously mentioned. The work accompanying the KD OMP was beneficial for its clear discussion of theoretical issues and its extensive and comprehensive tables of available experimental data.

A. A new potential

Our complex phenomenological optical model potential contains the traditional volume (V), surface (S), and spin-orbit (SO) nuclear terms which are delineated using the standard Woods-Saxon form factors

$$f_{WS}(r, \mathcal{R}_i, \mathcal{A}_i) = (1 + \exp((r - \mathcal{R}_i)/\mathcal{A}_i))^{-1}, \qquad (1)$$

[*]weppnesp@eckerd.edu
[†]Present address: Department of Physics, Florida State University, Tallahassee, FL 32306, USA.
[‡]Present address: Marine Technology Department, Rosenstiel School of Marine and Atmospheric Science, University of Miami, Miami, FL 33149, USA.
[§]Present address: Department of Physics, Georgia Institute of Technology, Atlanta, GA 30332, USA.

where $\mathcal{R}_i$ is the radius parameter and $\mathcal{A}_i$ is the geometric diffusive parameter. The i is a placeholder index for the V (volume), S (surface), and SO (spin orbit) designations. The phenomenological optical model potential takes the standard form

$$\begin{aligned}
&\mathcal{U}(r, E, A, N, Z, \mathcal{P}, MN) \\
&\quad = -\mathcal{V}_V(E, A, N, Z, \mathcal{P}, MN) f_{WS}(r, \mathcal{R}_V, \mathcal{A}_V) \\
&\qquad - i\mathcal{W}_V(E, A, N, Z, \mathcal{P}, MN) f_{WS}(r, \mathcal{R}_V, \mathcal{A}_V) \\
&\qquad + 4\mathcal{A}_S \mathcal{V}_D(E, A) \frac{d}{dr} f_{WS}(r, \mathcal{R}_S, \mathcal{A}_S) \\
&\qquad + i4\mathcal{A}_S \mathcal{W}_D(E, A, N, Z, \mathcal{P}) \frac{d}{dr} f_{WS}(r, \mathcal{R}_S, \mathcal{A}_S) \\
&\qquad + \frac{2}{r} \mathcal{V}_{SO}(E, A, N, Z, \mathcal{P}) \frac{d}{dr} f_{WS}(r, \mathcal{R}_{SO}, \mathcal{A}_{SO})(\mathbf{l} \cdot \sigma) \\
&\qquad + i \frac{2}{r} \mathcal{W}_{SO}(E, A, N, Z, \mathcal{P}) \frac{d}{dr} f_{WS}(r, \mathcal{R}_{SO}, \mathcal{A}_{SO})(\mathbf{l} \cdot \sigma) \\
&\qquad + f_{\text{coul}}(r, \mathcal{R}_C, A, N, Z, \mathcal{P}), \qquad (2)
\end{aligned}$$

where the $\mathcal{V}_i$ and $\mathcal{W}_i$ are the real and imaginary potential amplitudes, respectively, and f_{coul} is the Coulomb term which has the following traditional format:

$$\begin{aligned}
f_{\text{coul}}(r, \mathcal{R}_C, A, N, Z, \mathcal{P}) &= \frac{1+\mathcal{P}}{2} \frac{Ze^2}{r}, \\
r &\geqslant \mathcal{R}_C, \qquad (3) \\
f_{\text{coul}}(r, \mathcal{R}_C, A, N, Z, \mathcal{P}) &= \frac{1+\mathcal{P}}{2} \frac{Ze^2}{2\mathcal{R}_C} \left(3 - \frac{r^2}{\mathcal{R}_C{}^2}\right), \\
r &\leqslant \mathcal{R}_C. \qquad (4)
\end{aligned}$$

For a neutron projectile this term is set to zero. The amplitudes, radii, and diffusive parameters have the following dependent variables:

(i) **E**—projectile nucleon laboratory energy in MeV
(ii) **A**—Atomic number of the target nucleus
(iii) **N**—Number of neutrons in the target nucleus
(iv) **Z**—Number of protons in the target nucleus
(v) $\mathcal{P}$—+1 if projectile is a proton, −1 if a neutron
(vi) **MN**—set to 1 if the target is traditionally singly magic
—set to 2 if the target is traditionally doubly magic
—otherwise set to 0.

Explicitly the 13 Woods-Saxon terms of this OMP are given using 23 distinct parameters where one Woods-Saxon potential term may have up to three of these parameters. The systematic polynomial formats of these terms are described below. The parameters are purposely labeled to emphasize that each was fitted independently in the process of arriving at the final WP OMP, the techniques used will be detailed in Sec. III.

Here are the polynomial forms of this optical potential beginning with the volume amplitudes:

$$\begin{aligned}
\mathcal{V}_V &= V_{V_0} + V_{V_1} A + V_{V_2} A^2 + V_{V_3} A^3 + V_{V_5} E \\
&\quad + V_{V_6} E^2 + V_{V_7} E^3 \qquad (5) \\
&\quad + \mathcal{P}(N-Z)\left(V_{V_{i0}} + V_{V_{i1}} A + V_{V_{i2}} A^2 + V_{V_{i3}} A^3\right. \\
&\quad \left. + V_{V_{i4}} A^4 + V_{V_{i5}} E + V_{V_{i6}} E^2\right) \qquad (6) \\
&\quad + MN\left(V_{V_{m0}} + V_{V_{m1}} A + V_{V_{m2}} A^2 + V_{V_{m3}} A^3\right. \\
&\quad \left. + V_{V_{m5}} E + V_{V_{m6}} E^2\right), \qquad (7) \\
\mathcal{W}_V &= W_{V_0} + W_{V_1} A + W_{V_2} A^2 + W_{V_3} A^3 + W_{V_5} E \\
&\quad + W_{V_6} E^2 + W_{V_7} E^3 \qquad (8) \\
&\quad + \mathcal{P}(N-Z)\left(W_{V_{i0}} + W_{V_{i1}} A + W_{V_{i2}} A^2 + W_{V_{i3}} A^3\right. \\
&\quad \left. + W_{V_{i4}} A^4 + W_{V_{i5}} E + W_{V_{i6}} E^2\right) \qquad (9) \\
&\quad + MN\left(W_{V_{m0}} + W_{V_{m1}} A + W_{V_{m2}} A^2 + W_{V_{m3}} A^3\right. \\
&\quad \left. + W_{V_{m5}} E + W_{V_{m6}} E^2\right). \qquad (10)
\end{aligned}$$

The surface amplitudes are

$$\begin{aligned}
\mathcal{V}_S &= V_{S_0} + V_{S_1} A + V_{S_2} A^2 + V_{S_3} A^3 + V_{S_5} E \\
&\quad + V_{S_6} E^2 + V_{S_7} E^3, \qquad (11) \\
\mathcal{W}_S &= W_{S_0} + W_{S_1} A + W_{S_2} A^2 + W_{S_3} A^3 + W_{S_5} E \\
&\quad + W_{S_6} E^2 + W_{S_7} E^3 \qquad (12) \\
&\quad + \mathcal{P}(N-Z)\left(W_{S_{i0}} + W_{S_{i1}} A + W_{S_{i2}} A^2 + W_{S_{i3}} A^3\right. \\
&\quad \left. + W_{S_{i4}} A^4 + W_{S_{i5}} E + W_{S_{i6}} E^2\right). \qquad (13)
\end{aligned}$$

The spin orbit amplitudes are

$$\begin{aligned}
\mathcal{V}_{SO} &= V_{SO_0} + V_{SO_1} A + V_{SO_2} A^2 + V_{SO_3} A^3 + V_{SO_5} E \\
&\quad + V_{SO_6} E^2 + V_{SO_7} E^3 \qquad (14) \\
&\quad + \mathcal{P}(N-Z)\left(V_{SO_{i0}} + V_{SO_{i1}} A + V_{SO_{i2}} A^2\right. \\
&\quad \left. + V_{SO_{i3}} A^3 + V_{SO_{i4}} A^4 + V_{SO_{i5}} E + V_{SO_{i6}} E^2\right), \qquad (15) \\
\mathcal{W}_{SO} &= W_{SO_0} + W_{SO_1} A + W_{SO_2} A^2 + W_{SO_3} A^3 + W_{SO_5} E \\
&\quad + W_{SO_6} E^2 + W_{SO_7} E^3 \qquad (16) \\
&\quad + \mathcal{P}(N-Z)\left(W_{SO_{i0}} + W_{SO_{i1}} A + W_{SO_{i2}} A^2\right. \\
&\quad \left. + W_{SO_{i3}} A^3 + W_{SO_{i4}} A^4 + W_{SO_{i5}} E + W_{SO_{i6}} E^2\right). \qquad (17)
\end{aligned}$$

The volume radius and diffusive terms are

$$\begin{aligned}
\mathcal{R}_V &= R_{V_0} + R_{V_1} A + R_{V_2} A^2 + R_{V_3} A^3 + R_{V_5} E \\
&\quad + R_{V_6} E^2 + R_{V_7} E^3, \qquad (18) \\
\mathcal{A}_V &= A_{V_0} + A_{V_1} A + A_{V_2} A^2 + A_{V_3} A^3 + A_{V_5} E \\
&\quad + A_{V_6} E^2 + A_{V_7} E^3 \qquad (19) \\
&\quad + \mathcal{P}(N-Z)\left(A_{V_{i0}} + A_{V_{i1}} A + A_{V_{i2}} A^2 + A_{V_{i3}} A^3\right. \\
&\quad \left. + A_{V_{i5}} E + A_{V_{i6}} E^2 + A_{V_{i7}} E^3\right). \qquad (20)
\end{aligned}$$

The surface radius and diffusive terms are

$$\begin{aligned}
\mathcal{R}_S &= R_{S_0} + R_{S_1} A + R_{S_2} A^2 + R_{S_3} A^3 + R_{S_5} E \\
&\quad + R_{S_6} E^2 + R_{S_7} E^3, \qquad (21) \\
\mathcal{A}_S &= A_{S_0} + A_{S_1} A + A_{S_2} A^2 + A_{S_3} A^3 + A_{S_5} E \\
&\quad + A_{S_6} E^2 + A_{S_7} E^3, \qquad (22)
\end{aligned}$$

the spin-orbit radius and diffusive terms are

$$\begin{aligned}
\mathcal{R}_{SO} &= R_{SO_0} + R_{SO_1} A + R_{SO_2} A^2 + R_{SO_3} A^3 + R_{SO_5} E \\
&\quad + R_{SO_6} E^2 + R_{SO_7} E^3 \qquad (23) \\
&\quad + \mathcal{P}(N-Z)\left(R_{SO_{i0}} + R_{SO_{i1}} A + R_{SO_{i2}} A^2 + R_{SO_{i3}} A^3\right. \\
&\quad \left. + R_{SO_{i5}} E + R_{SO_{i6}} E^2 + R_{SO_{i7}} E^3\right), \qquad (24)
\end{aligned}$$

TABLE I. Model parameters for the subject of this work, the WP global optical potential Each term is a 5 to 7 term separable polynomial in A are E which are given in Eqs. (5)–(27). Tools have been developed to facilitate the use of this potential including an on-line optical potential calculator [11].

Term	0	1 (A)	2 (A^2)	3 (A^3)	4 (A^4)	5 (E)	6 (E^2)	7 (E^3)
V	$+5.703 \times 10^{+1}$	$+4.099 \times 10^{-1}$	-8.656×10^{-3}	$+5.793 \times 10^{-5}$	–	-5.881×10^{-1}	$+1.822 \times 10^{-3}$	–
V_i	$-7.810 \times 10^{+0}$	$+1.054 \times 10^{+0}$	-4.616×10^{-2}	$+8.384 \times 10^{-4}$	-5.416×10^{-6}	-6.729×10^{-3}	$+3.684 \times 10^{-5}$	–
V_m	-3.723×10^{-1}	$+6.563 \times 10^{-3}$	-5.308×10^{-4}	$+7.987 \times 10^{-6}$	–	$+2.515 \times 10^{-3}$	-5.607×10^{-6}	–
W	$-1.897 \times 10^{+0}$	-1.843×10^{-1}	$+5.034 \times 10^{-3}$	-3.814×10^{-5}	–	$+2.367 \times 10^{-1}$	-1.423×10^{-3}	2.556×10^{-6}
W_i	$+8.216 \times 10^{+0}$	-8.359×10^{-1}	$+3.221 \times 10^{-2}$	-5.426×10^{-4}	$+3.320 \times 10^{-6}$	$+8.446 \times 10^{-3}$	-2.644×10^{-5}	–
W_m	$-3.781 \times 10^{+0}$	$+1.818 \times 10^{-1}$	-4.772×10^{-3}	$+3.374 \times 10^{-5}$	–	$+4.157 \times 10^{-2}$	-2.149×10^{-4}	–
V_S	-4.612×10^{-1}	-1.178×10^{-2}	$+9.658 \times 10^{-4}$	-1.270×10^{-5}	–	$+7.906 \times 10^{-3}$	-4.230×10^{-5}	–
W_S	$+6.189 \times 10^{+0}$	$+1.740 \times 10^{-1}$	-4.790×10^{-3}	$+3.670 \times 10^{-5}$	–	-6.423×10^{-2}	-3.753×10^{-4}	$+3.096 \times 10^{-6}$
W_{S_i}	$+3.471 \times 10^{+0}$	-4.265×10^{-1}	$+1.670 \times 10^{-2}$	-2.828×10^{-4}	$+1.744 \times 10^{-6}$	$+1.449 \times 10^{-2}$	-8.093×10^{-5}	–
V_{SO}	$+1.562 \times 10^{+1}$	-1.202×10^{-1}	$+1.765 \times 10^{-3}$	–	–	-1.923×10^{-1}	$+1.168 \times 10^{-3}$	$+2.400 \times 10^{-6}$
V_{SO_i}	$-3.666 \times 10^{+0}$	$+7.228 \times 10^{-1}$	-3.524×10^{-2}	$+6.493 \times 10^{-4}$	-4.151×10^{-6}	$+2.472 \times 10^{-3}$	-3.317×10^{-6}	–
W_{SO}	$+3.929 \times 10^{-1}$	$+1.660 \times 10^{-1}$	-5.369×10^{-3}	$+4.646 \times 10^{-5}$	–	-3.702×10^{-2}	$+9.223 \times 10^{-5}$	–
W_{SO_i}	$+5.399 \times 10^{+0}$	-4.639×10^{-1}	$+1.718 \times 10^{-2}$	-2.809×10^{-4}	$+1.696 \times 10^{-6}$	-1.720×10^{-2}	$+1.234 \times 10^{-4}$	–
R_V	$+1.491 \times 10^{+0}$	-1.971×10^{-2}	$+5.447 \times 10^{-4}$	-4.561×10^{-6}	–	-6.255×10^{-3}	$+9.064 \times 10^{-5}$	-3.187×10^{-7}
A_V	$+1.933 \times 10^{-1}$	$+3.484 \times 10^{-2}$	-9.172×10^{-4}	$+6.999 \times 10^{-6}$	–	$+5.762 \times 10^{-3}$	-6.097×10^{-5}	$+1.929 \times 10^{-7}$
A_{V_i}	$+2.207 \times 10^{-3}$	$+5.253 \times 10^{-3}$	-1.970×10^{-4}	$+2.043 \times 10^{-6}$	–	-5.014×10^{-4}	$+1.898 \times 10^{-6}$	–
R_S	$+8.599 \times 10^{-1}$	-5.657×10^{-3}	$+8.884 \times 10^{-5}$	$+7.253 \times 10^{-7}$	–	$+1.024 \times 10^{-2}$	-4.166×10^{-5}	–
A_S	$+9.477 \times 10^{-1}$	$+5.097 \times 10^{-3}$	$+1.201 \times 10^{-4}$	-2.824×10^{-6}	–	-1.255×10^{-2}	$+4.597 \times 10^{-5}$	–
R_{SO}	$+8.293 \times 10^{-1}$	$+3.098 \times 10^{-2}$	-7.747×10^{-4}	$+6.035 \times 10^{-6}$	–	-3.894×10^{-3}	$+1.799 \times 10^{-5}$	–
R_{SO_i}	-1.132×10^{-1}	-5.916×10^{-4}	$+3.596 \times 10^{-6}$	–	–	$+4.458 \times 10^{-3}$	-4.652×10^{-5}	$+1.521 \times 10^{-7}$
A_{SO}	$+9.239 \times 10^{-1}$	$+3.091 \times 10^{-2}$	-7.702×10^{-4}	$+5.982 \times 10^{-6}$	–	-1.874×10^{-2}	$+1.576 \times 10^{-4}$	-4.161×10^{-7}
R_C	$+3.604 \times 10^{+0}$	-2.103×10^{-1}	$+7.753 \times 10^{-3}$	-8.155×10^{-5}	–	$+1.074 \times 10^{-1}$	-6.348×10^{-4}	–
R_{C_i}	$+3.404 \times 10^{-1}$	-1.038×10^{-1}	$+1.294 \times 10^{-3}$	–	–	$+4.501 \times 10^{-2}$	-3.729×10^{-4}	$+9.467 \times 10^{-7}$

$$\mathcal{A}_{SO} = A_{SO_0} + A_{SO_1}A + A_{SO_2}A^2 + A_{SO_3}A^3 + A_{SO_5}E + A_{SO_6}E^2 + A_{SO_7}E^3, \tag{25}$$

and finally the Coulomb radius term is

$$\mathcal{R}_C = R_{C_0} + R_{C_1}A + R_{C_2}A^2 + R_{C_3}A^3 + R_{C_5}E + R_{C_6}E^2 + R_{C_7}E^3 \tag{26}$$

$$+ \mathcal{P}(N-Z)\left(\frac{2Z}{A}\right)^{\frac{1}{3}}\left(R_{C_{i0}} + R_{C_{i1}}A + R_{C_{i2}}A^2 + R_{C_{i3}}A^3 + R_{C_{i4}}A^4 + R_{C_{i5}}E + R_{C_{i6}}E^2 + R_{C_{i7}}E^3\right). \tag{27}$$

Parameters in this OMP which are at variance with the other OMPs are the real surface amplitude [Eq. (11)] (which is small), imaginary asymmetry $(N-Z)$ [Eqs. (9), (13), (17)], geometric asymmetry [Eqs. (20), (24), (27)], and the magic number dependent terms [Eqs. (7), (10)]. The asymmetric parameters and their ramifications are discussed in Sec. V. The magic number terms attempt to better characterize the bonding that occurs in these closed shell nuclei. Our short term Coulomb radius is also untraditionally energy dependent, the rational for this will be discussed in Sec. V. The 23 parameters, of Eqs. (5)–(27), which describe the 13 potential terms of Eq. (2), are listed in Table I.

This potential was put into a standard optical potential calculator which solves the Schrödinger equation for spin $\frac{1}{2}$-spin 0 scattering using a distorted Born wave approximation (DWBA) in a Coulomb wave function basis. TALYS [13,14] was used which applies ECIS [15] to calculate the solution once the final product was developed. We have produced a Java applet [11] which contains our own optical potential calculator as well as some useful input files for use in TALYS and ECIS which will let researchers produce results quickly. The gestation of the parameters will be described in Sec. III but first an overview will be given of the theoretical structure of this and the other recent global OMPs.

B. Theoretical comparison with other global optical potentials

The general design of all three OMPs under study (KD [1], MD [2], WP) is the same. They use similar Woods-Saxon functional forms which include volume and spin-orbit terms. Additionally the KD and WP optical potentials include surface terms. The KD and MD potentials also include an additional Coulomb correction term, in the WP optical potential the short term Coulomb potential includes energy dependence to include these Coulomb correction effects (this will be discussed in great detail in Sec. V B). Both the WP and MD produce one potential that is utilized for both proton and neutron scattering while the KD potential has separate potentials for the isospin dependence of the projectile.

The KP OMP [1] imaginary parameters are determined by a dispersive relationship which is dependant on the difference between the projectile laboratory energy and the Fermi energy of the target potential as well as constants designated as part of the real potential. Of the three optical potentials discussed it has the deepest theoretical underpinnings and given these

dispersive constraints and high accuracy it has successfully pushed the theoretical development of the global optical model potential to a new level.

A goal of the MD OMP [2] is to describe the elastic scattering data sets using fewer parameters. It uses constants, linear, and the occasional quadratic forms to describe all of its Woods-Saxon parameters. It is quite impressive that a high quality isospin dependent potential was produced with so few parameters.

In contrast this work (WP OMP) uses quadratic, cubic, and occasionally quartic polynomials that have no direct relationship to formal scattering theory. It has the highest amount of adjustable parameters of the three potentials. What it achieves is ease of use, good asymmetry and mirror nuclei analysis, and complete separability between the nucleon (A) and energy (E) parameters. This WP potential also includes a direct imaginary vector isospin asymmetry ($N - Z$) terms which neither of the other potentials have. In Sec. V a detailed comparison of the isovector differences of these three optical potentials will ensue.

III. PROCEDURE

This research tried ambitiously to minimize a χ^2 (proportional to the square of the difference between the theoretical fit and the experimental data). On over 300 different nucleon-nucleus experiments by adjusting the polynomial fit to the 23 parameters given in Table I. To attempt to decouple the terms from each other, the 23 values were varied using a systematic method detailed below. A listing and discussion of the experimental data set used to constrict the variables then follows.

A. Calculation techniques

The fitting elastic nucleon-nucleus scattering code was developed by two of the authors (S.W. and R.P.). A Numerov routine found in Ref. [12] was used to solve the nonrelativistic position space Schrödinger equation in a Coulomb basis with a relativistic correction found in Ref. [5]. The routine which produced the Coulomb wave functions was found in Ref. [16]. A Powell routine, adopted from Numerical Recipes [17], was used to minimize a weighted χ^2.

The code was developed to run on a multiprocessor parallel system. Each processor was assigned at least one nucleon-nucleus experimental data set at a given energy (E) and nucleon number (A). This data set could be as simple as one experiment or many experiments including the observables of total neutron cross section, total reaction cross section, differential cross section, and polarization. Each set contained, if available, both proton and neutron observables and varying target proton numbers that all shared a common target nucleon number and projectile energy. For example $A = 40$, $E = 40$ MeV experimental data exists for a proton striking ^{40}Ca and producing a total reaction cross section observable, a differential cross section, and polarization. These were fit simultaneously with data that exists for a neutron striking ^{40}Ca and producing a differential cross section, a total reaction cross section, a total cross section, and finally also including a proton at 40 MeV striking ^{40}Ar and producing a reaction and differential cross section. All eight of these experiments made a complete working data set in which the parameters were varied and the minimization routine for the weighted χ^2 was executed. By analyzing many different data sets together at the same energy and nucleon number it was intended to reduce systematic error and ultimately derive a better global fit among chains of target nuclei.

Each fitting cycle was comprised of a three step process. First all parameters were adjusted except three [the two magic number and the asymmetry Coulomb parameters: Eqs. (7), (10), (27) were held fixed]. Since the other 20 parameters were being adjusted simultaneously it was important to analyze only a subset of the entire experimental data set to avoid ambiguities within the parameter space. The data sets used encompassed either only $N = Z$ targets or certain sets in which a variety of different Z targets existed for a fixed nucleon number and fixed projectile energy or certain sets in which both neutron and proton projectile observables existed for that fixed A and fixed projectile energy E. These sets therefore either had zero $N - Z$ dependence or this dependence was clearly delineated by including a variety of elements as targets and/or projectiles. There were 115 data sets of fixed E and A experiments on which these 20 parameters were allowed to vary while searching for a minimum weighted χ^2. The best values for the parameters were then fit to the polynomials of A and E listed in Eqs. (5)–(27).

Second all data sets with nonzero ($N - Z$) dependence were used to adjust 13 parameters. There were thus ten parameters held fixed which were the nonasymmetric potential parameters that had other asymmetric terms within the same Woods-Saxon potential term [Eqs. (5), (8), (12), (14), (16), (19), (23), (26) and the magic number terms Eqs. (7), (10) were held fixed], the other 13 terms were varied. There were 90 experiment data sets (each data set might contain more than one experiment as detailed above) with some $N - Z$ dependences that were used for this task. The best values for the parameters were then fit to the polynomials in A and E. The parameters that were free to be modified in both of these steps were deduced using an average of both values which produced the minimum weighted χ^2 results.

Lastly, the magic number terms were adjusted [Eqs. (7), (10) were varied] to find the minimum weighted χ^2 keeping all other parameters fixed. For the magic numbers the traditional 2, 8, 20, and 28 were used. There were 40 data sets which contained at least one target magic nuclei experiment which were used to constrain these last two parameters.

The variances in the parameters were minimized to a weighted χ^2 which favored forward angles over backward angles (in the χ calculation there was a square root relationship such that the 50th forward angle point in a differential cross section was weighted only about one-seventh that of the extreme forward point following Ref. [3]). Differential cross sections were favored over polarizations by a factor of 1.5 and in general neutron total cross section point were favored to be approximately equal to half of a complete typical differential cross section. Used, but favored at half the weighting of the total neutron cross section, were the neutron and proton reaction cross sections. Choosing the correct weightings was

TABLE II. This is a partial listing of the proton-nucleus experimental data used in the fitting process of this work, the remainder is located in Table 7 of Ref. [1]. The references are listed followed by the laboratory energy of the projectile and the observables found in the reference article (rcs—total reaction cross section, dcs—differential cross section, pol—analyzing power). The data has an energy range from 30 MeV to 160 MeV, and a nucleon number, $12 \leqslant A \leqslant 60$ as required by the calculation. Table 7 of Ref. [1] contains* a substantial listing of experimental data references primarily for the ^{27}Al, ^{28}Si, ^{40}Ca, ^{54}Fe, ^{56}Fe, ^{58}Ni, and ^{60}Ni, all those experimental references were also used in this work if they were within this optical potentials applicable energy range.

Proton-Nucleus Experimental Elastic and Total Reaction Data References

Nucl.	[Ref] (Energies (MeV); Observables)	Nucl.	[Ref] (Energies (MeV); Observables)	Nucl.	[Ref] (Energies (MeV); Observables)
^{12}Be	[19](55;dcs)	^{12}C	[20](20-84;dcs,pol) [21](30;dcs,pol)	^{13}C	[21](30;dcs,pol) [22](35;dcs)
^{14}N	[23](30;dcs) [22](35;dcs)		[24](30-60;rcs) [22](35;dcs)		[25](35;dcs,pol)
	[23,26](50;dcs,pol) [27](35;rcs)		[28](35;dcs) [29](40;dcs)		[30,31](72;dcs,pol)
	[32](122;dcs) [33](142;dcs)		[34](49;dcs) [35](50;dcs)		[36](135;dcs,pol)
^{15}N	[22](35;dcs) [37](39,44;dcs)		[38](61;dcs) [39](65;dcs,pol)	^{16}O	[21](30;dcs,pol) [40](35;dcs,pol)
	[41](42,44;dcs) [31](65;dcs,pol)		[42](65;rcs) [43](75,150;dcs,pol)		[22,37](35;dcs) [44](30-47;rcs)
^{17}O	[22](35;dcs) [45](66;dcs)		[46](81-180;rcs) [47](96,dcs)		[48](43,46;dcs)
^{18}O	[22](35;dcs) [41](42,44;dcs)		[49](122,160;dcs,pol)		[26,35](49;dcs,pol)
	[50](43;dcs) [45](67;dcs)		[51](135;dcs,pol,rcs)		[52](65;dcs,pol) [42](65;rcs)
^{20}O	[53](30;dcs) [50](43;dcs)		[54](142;dcs) [55](145;dcs,pol)		[56](135;dcs,pol)
^{20}Ne	[22](35;dcs) [27](35;rcs)		[31](150;dcs pol)	^{22}O	[57](47;dcs)
	[52](65;dcs,pol)		[58](156;dcs,pol)	^{22}Ne	[22,37](35;dcs)
^{24}Mg	[59](30-45;dcs) [60](50;dcs,pol)	^{28}Si*	[61](52;dcs)	^{29}Si	[30](72;dcs,pol)
	[39,52](65;dcs,pol)	^{30}Si	[62](52;dcs)	^{31}P	[30](72;dcs,pol)
	[63](80;dcs,pol) [64](135;dcs,pol)	^{32}Si	[65](42;dcs)	^{32}S	[66](53;dcs) [39](65;dcs,pol)
^{34}S	[67](30;dcs)	^{34}Ar	[66](47;dcs)	^{36}Ar	[68](33;dcs)
^{37}Cl	[22,37](35;dcs)	^{39}K	[22,37](35;dcs)	^{40}Ar	[69](30,33,37,41;dcs,pol)
^{40}Ca*	[46](80-180;rcs) [70](30-48;dcs)	^{42}Ar	[68](33;dcs)		[22,23,37](30-50;dcs,pol)
^{42}Ca	[70](30-48;dcs) [71](30-48;rcs)	^{44}Ar	[68](33;dcs)		[27](36-47;rcs) [52](65;dcs,pol)
	[22](35;dcs) [72](49;dcs)	^{44}Ca	[70](30-48;dcs) [71](30-48;rcs)	^{45}Sc	[37](35;dcs) [72](50;dcs,pol)
	[73](65;dcs,pol)		[72](49;dcs) [52,74](65;dcs,pol)	^{46}Ti	[52,73](65;dcs,pol) [75](100;dcs)
^{48}Ca	[70](30-48;dcs) [71](30-48;rcs)	^{48}Ti	[76](30-48;rcs)	^{50}Ti	[73](65;dcs,pol) [75](100;dcs)
	[52,73,74](65;dcs,pol)		[52,73](65;dcs,pol) [75](100;dcs)	^{50}Cr	[61](52;dcs) [73]
^{52}Cr	[73](65;dcs;pol)		[77](100;rcs)	^{54}Cr	[22](35;dcs) [73](65;dcs;pol)
^{54}Fe*	[78](30,40,62;dcs)		[58](156;dcs)	^{56}Fe*	[24](40,60;rcs) [79](65;dcs,pol)
	[80](30-48;rcs) [81](40;dcs,pol)	^{58}Fe	[22](35;dcs)	^{59}Co	[82](30;dcs) [83](40;dcs)
					[80](30,40;rcs) [84](65;dcs,pol)

found to be an art form where a balance tenuously existed in which every reaction was regarded but certain reactions were strengthened so that the χ^2 parameter space contained large relative minima which the search functions could find easily.

To find these minima a Monte Carlo preliminary gross search was done using a Sobol [18] number generator. Since the parameter space was often twenty dimensions this might include up to 3×10^5 vectors in which weighted χ^2 were first calculated by solving the Schrödinger equation for the given potential. The lowest ten vectors were analyzed in finer detail by seeking the local minima in their vicinity within the χ^2 parameter space. The χ^2 minimization program sought the steepest derivative in the multidimensional parameter space [17]. Although the overall quality of the fits were examined occasionally, the entire process was close to automatic.

At first the 23 parameters had large variances which were slowly reduced following the three steps described as the weighted normalized per point chi-squared was reduced and approached a global minimum gracefully. The highest 5% of the χ^2 were thrown out after each fit (which routinely were the same sets) and then each parameter was fit originally to a cubic polynomial in A (nucleon number) and E (projectile energy). Eventually many of the cubics were reduced to quadratics if warranted and in the asymmetry terms the A polynomial was increased to fourth order to give a better fit over the entire nucleon target atomic number range.

B. Experimental data sets

This work strived for a comprehensive collection of experimental data sets. As a starting point the excellent summary of elastic data found in Ref. [1] was used, the product of the KD optical potential group. This was supplemented with new data and also nuclei outside the assumed range of the KD potential. These additional data sets were either nuclei lighter than ^{27}Al or those nuclei which are nonspherical and were not considered in that article, there were also a few additional data sets that were discovered and added to our database. All proton-nucleus data sets used that were not in Ref. [1] are listed in Table II. The smaller set of neutron-nucleus data sets used here and

TABLE III. This is a partial listing of the neutron-nucleus experimental data used in the fitting process of this work, the remainder is located in Table 1 of Ref. [1]. The references are listed followed by the laboratory energy of the projectile and the observables found in the reference article (rcs—total reaction cross section, dcs—differential cross section). The data has an energy range from 30 MeV to 160 MeV, and a nucleon number, $12 \leqslant A \leqslant 60$ as required by the calculation. Table 1 of Ref. [1] contains* a substantial listing of experimental data references primarily for ^{24}Mg, ^{27}Al, ^{28}Si, ^{32}S, ^{40}Ca, and ^{56}Fe, all those experimental references were also used in this work if they were within this optical potentials applicable energy range. The neutron total cross section data sets of Refs. [92,93] were also extensively used.

Neutron-Nucleus Experimental Elastic and Total Reaction Data References

Nucl.	[Ref] (Energies (MeV); Observables)	Nucl.	[Ref] (Energies (MeV); Observables)	Nucl.	[Ref] (Energies; (MeV) Observables)
^{12}C	[85](30-49;rcs) [86](35;dcs) [87](55-75;dcs) [88](65-156;dcs) [90](96;dcs) [89,91](misc.;rcs)	^{14}N	[85](30-49;rcs)	^{16}O	[85](30-49;rcs) [56](35;dcs)
		^{27}Al*	[85](30-49;rcs)	^{28}Si*	[89](misc.;rcs)
		^{40}Ca*	[85](30-49;rcs) [88](65-156;dcs)	^{56}Fe*	[89](misc.;rcs)

not cited in Ref. [1] are listed in Table III. A reader of this work, Ref. [1], and the growing EXFOR/CSISRS database at the National Nuclear Data Center [94] have a near complete compilation of elastic nucleon-nucleus and total cross section experimental data listings at intermediate energies.

Not all the experimental data were used to help constrain this OMP. Some data, usually published before 1960, had large systematic differences with later reactions and were disregarded. Also, as mentioned in Sec. III, calculations were only done if angular differential data existed at a given energy and nucleon number. It was established for this fitting procedure that total cross section data did not have enough information (only one data point) to constrain the parameters adequately so it was only used in conjunction with differential experimental data. Occasionally if the energy of a total reaction cross section was close to an energy where differential data existed, the total reaction cross section data was adjusted following the forms given in Refs. [95,96]. This procedure was not needed for the total neutron cross section data of Refs. [92,93] since the energy coverage was substantial for these data sets.

IV. RESULTS

To produce the calculations shown in this section the DWBA scattering code TALYS [13,14] was used for consistency. All experimental data are shown as black circles, the new results of this work are depicted as light solid green lines (WP OMP), the calculations of Koning and Delaroche [1] (KD OMP) are shown using dark blue dashed lines and the calculations of Madland [2] (MD OMP) are depicted using a medium red dot-dashed lines. The motivation is not to be exhaustive but to give a fair representative overview of the features of these three modern optical potentials. As a global summary it can be concluded that that all three potentials do a fairly good job fitting the presently available elastic scattering data and dramatic contrasts are not proffered until Sec. V. The details of this section do illustrate some minor differences and so first their will be an examination of the neutron-nucleus observables then following with the proton-nucleus observables.

A. Neutron-nucleus observables

In Figs. 1–4 the calculations of total neutron cross section results to the comprehensive data sets of Refs. [92,93] are compared. Overall the calculations of the KD OMP of Ref. [1] do the best job at reproducing the experimental data, usually within a remarkable 1%. The potential of this work (WP OMP) is usually within 5% of the experimental data sets and that of

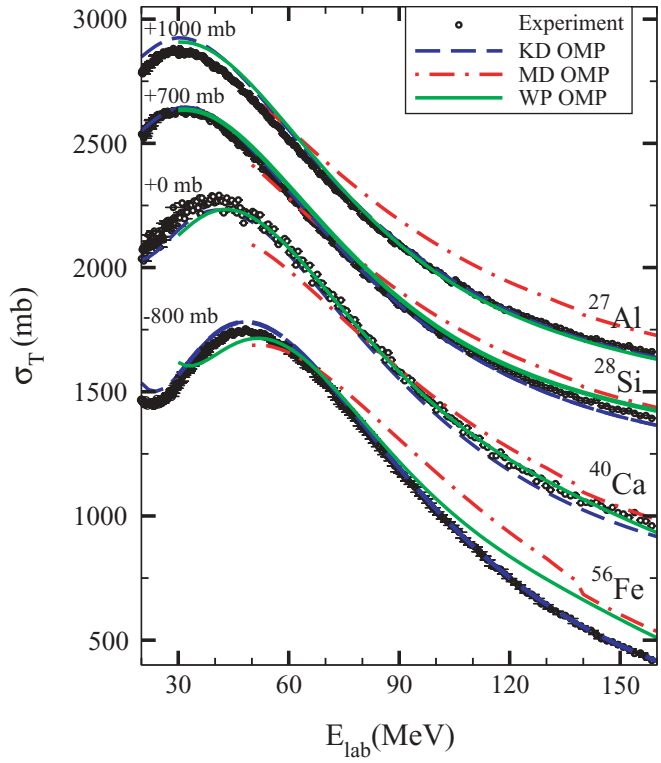

FIG. 1. (Color online) The experimental total cross section for neutrons scattering from ^{27}Al [92], ^{28}Si [92], ^{40}Ca [93], and ^{56}Fe [93] from 20 MeV to 160 MeV for the laboratory energy of the neutron. They are fit to three different optical potential calculations (KD [1], MD [2], and to this work: WP) which are described in the legend. The experimental data and theory have been offset by constant amounts for multiple comparisons on one graph. The WP and MD calculations have a minimum energy limit of 30 and 50 MeV respectively.

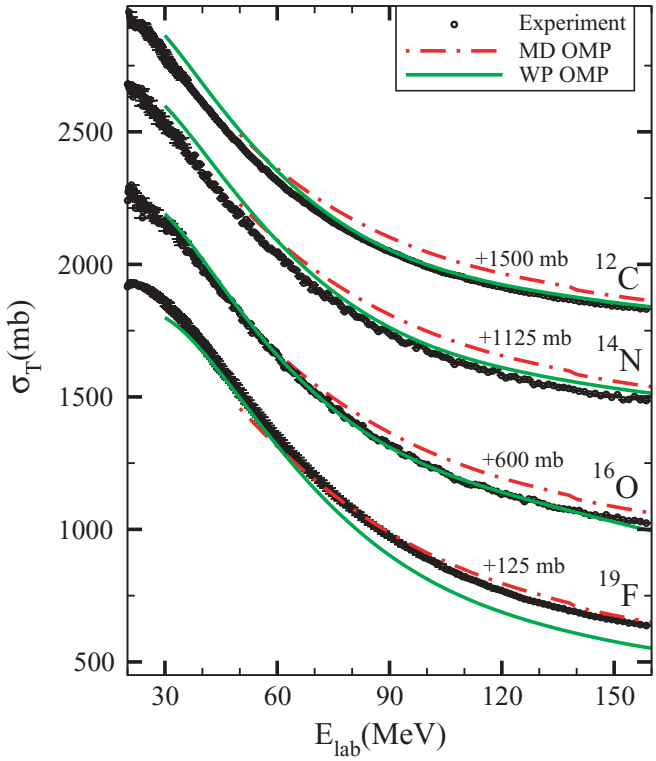

FIG. 2. (Color online) The experimental total cross section for neutrons scattering from the light nuclei of ^{12}C [93], ^{14}N [92], ^{16}O [92], and ^{19}F [93] from 20 MeV to 160 MeV for the laboratory energy of the neutron. They are fit to two different optical potential calculations (MD [2], and to this work: WP) which are described in the legend. The experimental data and theory have been offset by constant amounts for multiple comparisons on one graph. The WP and MD calculations have a minimum energy limit of 30 and 50 MeV respectively. The KD calculation is not applicable for these light nuclei.

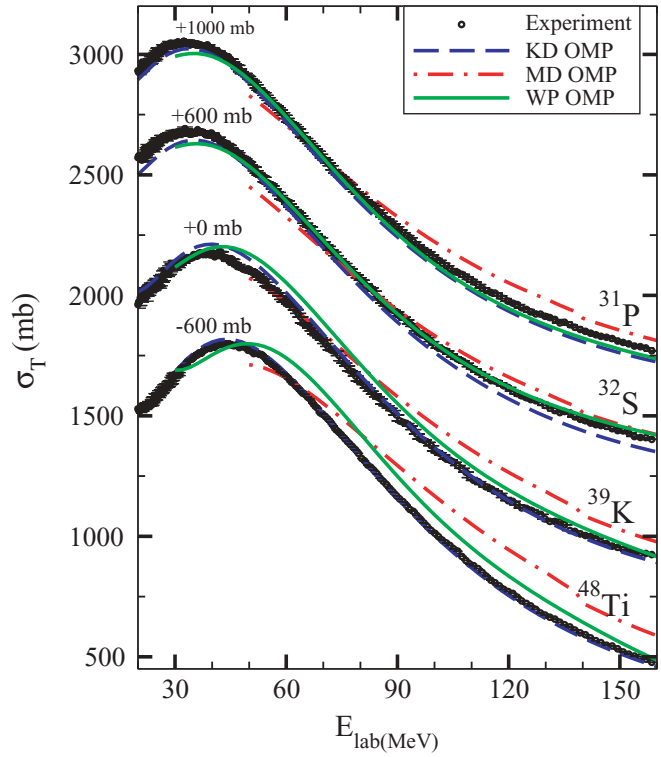

FIG. 3. (Color online) The experimental total cross section for neutrons scattering from ^{31}P [93], ^{32}S [93], ^{39}K [93], and ^{48}Ti [93] from 20 MeV to 160 MeV for the laboratory energy of the neutron. They are fit to three different optical potential calculations (KD [1], MD [2], and to this work: WP) which are described in the legend. The experimental data and theory have been offset by constant amounts for multiple comparisons on one graph. The WP and MD calculations have a minimum energy limit of 30 and 50 MeV respectively.

the MD OMP is usually within 10%. These are plotted on an elongated linear scale to accentuate the disparity but it should be recognized that even a 10% difference between theory and experiment is extraordinary for most nuclear scattering observables.

The remarkable fit by the KD OMP calculation is justified, the authors considered these data important and thus weighted them accordingly. They also had, as discussed in Sec. II, a separate proton nucleus and neutron nucleus potential. At energies greater than 50 MeV, where neutron-nucleus elastic scattering data are scarce, this was one of the few observables used to fit their neutron optical potential. With fewer constraints this observable, with its high caliber of data [92,93], was easier to fit. Conversely the optical potential of this work and the optical potential of the MD OMP had to continually compromise by both fitting neutron-nucleus and proton-nucleus observables simultaneously.

In Fig. 1 the calculations are fit to four standard nuclei. As in all these calculations the WP calculation of this work (solid green line) was not tested below 30 MeV and the MD calculation was not used below 50 MeV. Likewise the KD calculation is not applicable to the lighter nuclei ($A < 27$) targets. Systematic trends emerge where the KD calculation runs lower and closer to the experimental results than the other two calculations for the neutron-nucleus total cross section. The WP calculation is also systematically lower and closer than the MD calculation for the neutron total cross section observables as typified in this figure. There is a small kink in the MD results at $E = 130$ MeV, this is a real discontinuity in the Woods-Saxon function form parameters for this potential at both 130 MeV and 140 MeV. The history of the phenomenological fitting endeavor shows that researchers have struggled to fit these higher energies well, the present works are no exception.

Figure 2 contains the lighter targets which follow the same trends as described for Fig. 1. Of the two applicable optical potential calculations (the KD OMP is defined only when $A \geqslant 24$) the WP OMP of this work does better in all cases except for neutron scattering from ^{19}F. The odd nuclei have nonzero spin forces which are not included in the solution technique which in part may explain the anomaly.

Concluding the results of neutron-nucleus total cross section calculations are Figs. 3 and 4 which contain a variety of less common nuclei and odd spin nuclei neutron total cross sections. The KD optical potential of Ref. [1] which was explicitly not fit to these nonspherical nuclei still does

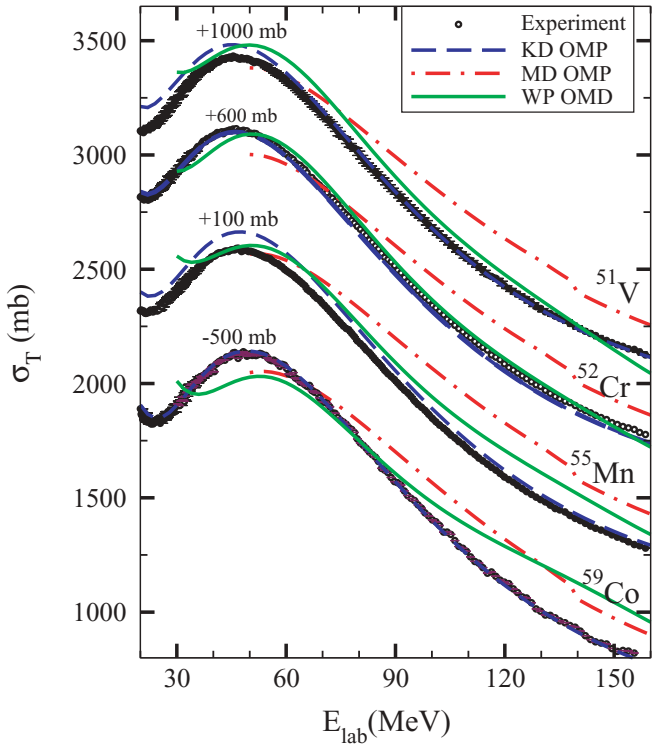

FIG. 4. (Color online) The experimental total cross section for neutrons scattering from ^{51}V [93], ^{52}Cr [93], ^{55}Mn [93], and ^{59}Co [93] from 20 MeV to 160 MeV for the laboratory energy of the neutron. They are fit to three different optical potential calculations (KD [1], MD [2], and to this work: WP) which are described in the legend. The experimental data and theory have been offset by constant amounts for multiple comparisons on one graph. The WP and MD calculations have a minimum energy limit of 30 and 50 MeV respectively.

remarkably well, the same trends discussed in the earlier figures still hold. What becomes apparent in the heavier nuclei ($50 \leqslant A \leqslant 60$) calculations of this work (WP OMP—solid light green line) is that there seems to be a systematic energy shift; the shape of the curve is good, but it seems to contain a small shift toward higher energies, a possible explanation will be proffered in Sec. V B.

The neutron-nucleus differential experimental data are scarce above 30 MeV (see Table III and Ref. [1]). A representative sample of the data with calculations is shown in Fig. 5. Overall, all three potentials describe the experimental data adequately, most impressive are the results of the calculation of the MD potential which simultaneously fits both proton-nucleus and neutron-nucleus data while also using the fewest terms and parameters of the three optical potentials examined. Systematically the WP potential of this work has the weakest results, especially when the scattering angle is greater than 45 degrees. This implies that to improve these results the WP potential would need to give more weighting to higher angle results than was determined (see Sec. III which discusses the weightings chosen). To adequately measure the effects and form of the isospin dependent and asymmetry terms in the optical potential which is used by the WP and MD OMPs more high energy neutron-nucleus differential and reaction data are sorely needed [101,102].

Overall the best optical potential calculation for neutron-nucleus scattering is the work of Koning and Delaroche (KD OMP) [1]. It has the best fit to the total cross section observables (even the nonspherical and odd nuclei which were not used to constrain that potential) and it also does an admirable job with the differential observables. It has a wide energy range and is thus suitable for systematic neutron-nucleus studies. Its largest deficit is that it is not applicable to light nuclei ($A < 24$) which are important in astrophysics and biological physics.

B. Proton-nucleus scattering observables

The proton-nucleus elastic scattering observables will now be considered. The potential used by the MD and WP calculations remains the same while the KD potential uses a different optical potential to calculate the proton-nucleus observables.

A representative sample of the inelastic or reaction total cross section data is shown in Fig. 6 with projectile energies ranging from 30 MeV to 160 MeV. The calculations in this case are not as close to the experimental data, and the data are much sparser and more unsure than the earlier neutron total cross section data. More accurate high energy data are needed in this observable to better constrain the optical model theory (it plays a significant role in determining the absorptive strength [46,103]), an example will be proffered to illustrate this in Sec. V. All three global optical potentials do well but are not excellent. As with the neutron total cross sections the legend is the same and the figure is elongated and plotted on a linear scale to emphasis the differences.

There is a much more substantial amount of experimental data for the proton-nucleus differential cross section and the spin observable analyzing power and a representative sample is contained in Figs. 7–13. In Fig. 7 there is a comparison of some of the common nuclei targets, ^{27}Al, ^{28}Si, and ^{40}Ca for the differential cross section normalized to the Coulomb Rutherford differential cross section. Then an examination of the heavier common target subset (^{54,56}Fe and ^{58}N) transpires in Fig. 8. All these nuclei were calculated in Ref. [1] by the KD calculation and in this work are compared with the MD and WP potentials (in the applicable energy ranges, an MD calculation is not created for an energy of the projectile of less than 50 MeV). Overall, all three calculations do well. Some systematic trends become apparent: the WP OMP struggles at the higher angles to reproduce the experimental data (as it did with the neutron-nucleus observables). The disappointing fit at larger angles insinuates that the balance of the weighting functions for the WP OMP favored the forward angles too much. The KD OMP often exaggerates the minimum which probably signifies that the Coulomb strength is slightly weak short range as prescribed in that potential (in general the long term Coulomb force mildly obscures the diffraction effect generated by the short term forces). Because these are plotted on a logarithmic scale the percent difference between the theory and experiment is often larger than it appears (sometimes as much as 50% compared to 10% for the total cross sections). The quality of fit, as ascertained by an analysis

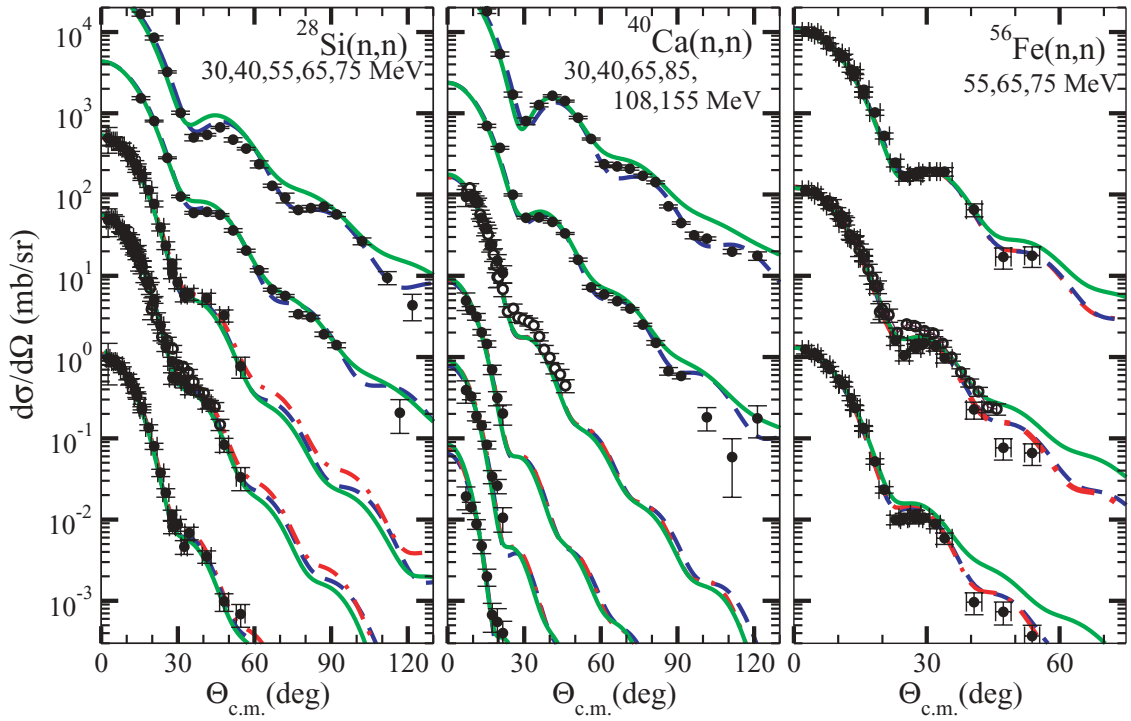

FIG. 5. (Color online) Neutron-nucleus elastic differential cross section experimental data for the target nuclei of ^{28}Si [87,97,98], ^{40}Ca [88,98,99], ^{56}Fe [87,97,98,100] at a variety of incident laboratory energies. They are fit to three different optical potential calculations (KD [1], MD [2], and to this work: WP). As in all figures, KD OMP is a blue dashed line, MD OMP is a red dot-dashed line and WP OMP is a green solid line. The experimental data and theory have been offset by constant amounts for multiple comparisons on one graph. The target labels at the top read left to right correspond to the calculations and experimental data read top to bottom. The MD calculations has a minimum energy limit of 50 MeV and is therefore missing from calculations below that energy.

of the χ^2 in Ref. [1], is not as good as with the neutron observables, yet it is still quite impressive for all three optical potentials.

The next two figures (Figs. 9 and 10) examine the reduced differential cross section of target nuclei which are nonspherical and farther from the line of stability than fit in Ref. [1] using the KD potential. Many of these examples are odd nonspin zero nuclei. Overall the three potentials do surprisingly well with the same systematic problem as with the more popular and common nuclear targets, however some aspects are dissatisfying. In Fig. 9 the results of the proton-nucleus reduced differential cross section of the calcium and chromium isotopes are shown and none of the calculations do extremely well describing all four isotopes simultaneously. The research of this work focused on trying to find the strength of the isovector antisymmetry term by simultaneously fitting these isotopes' observables together. The resulting calculation (the solid green line) fit ^{40}Ca and ^{44}Ca isotopes comfortably but struggle with the two other isotopes, the other calculations are in similar predicaments. The general shape is correct but the minima and maxima are often missed by over 25%. It seems that a asymmetry term which is linear and has mirror symmetry evades accurate discovery. The same difficulties with describing the calcium isotopes were recently discussed in Ref. [101]. These same arguments can be made, to a lesser extent, with chromium as shown in Fig. 9. The failure to create an excellent isovector asymmetry term is the motivation for the analysis of Sec. V. It also must be recognized that these potentials are often also missing a general spin-spin term which may be important for nonspin zero targets. As this potential was being developed a spin-spin term was used but the results had a substantial amount of noise and it was eventually removed. A competent analysis of the validity and strength of this spin-spin term would be a worthy endeavor for future work.

Figure 10 contains the reduced differential cross section of some lighter targets (if $A < 27$ the KD calculation is not applicable). This figure shows the struggles the calculations have to fit at higher energies which has been a common problem with an optical model calculation [49]. Likewise the back angles continually cause difficulty in the lighter targets. Recently there has been success in fitting these back angles by adding terms which add nonlocal approaches to these local OMPs [111,112] by adding angular momentum and parity dependencies to the potential.

In the center panel are highlighted some newer differential cross section data of the oxygen isotopes. The WP calculation (which is the only one applicable) does well in describing the general trend of the first diffraction minimum shifting as the neutron number increases. The mirror nuclei of calcium and argon are the targets in the right most panel. A recurring disappointment is not being able to fit all the isotopes with the same excellent quality of fit, an important motivation for this work. However, for those working with exotic beams,

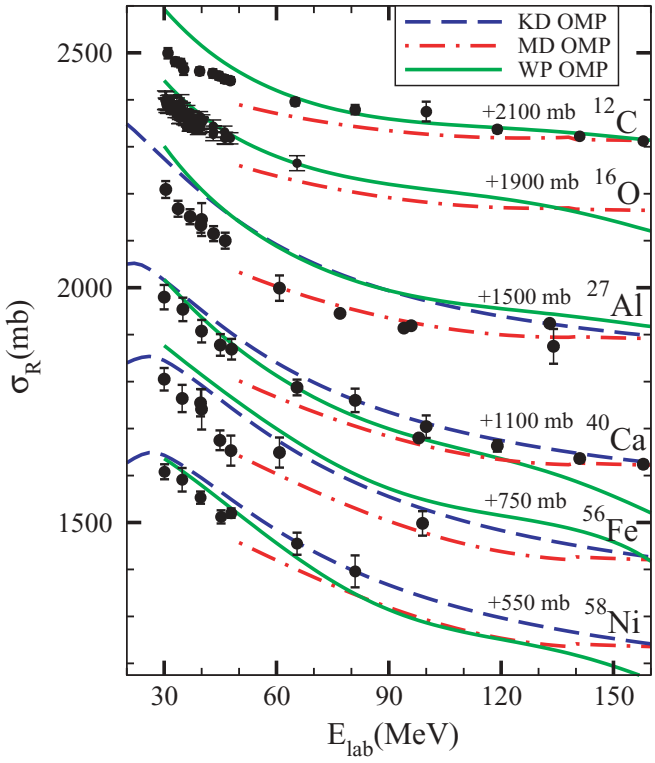

FIG. 6. (Color online) Proton-nucleus total inelastic cross section data for the targets ^{12}C, ^{16}O, ^{27}Al, ^{40}Ca, ^{56}Fe, and ^{58}Ni from 20 MeV to 160 MeV for the laboratory energy of the projectile proton. The experimental data comes from a variety of sources and are compiled and discussed in Refs. [1,77,95]. There are also new higher energy measurements for ^{12}C and ^{40}Ca found in Ref. [46]. They are fit to three different optical potential calculations (KD [1], MD [2], and to this work: WP) which are described in the legend. The experimental data and theory have been offset by constant amounts for multiple comparisons on one graph. The WP and MD calculations have a minimum energy limit of 30 and 50 MeV respectively.

this potential does give a good starting basis for continuing research.

In Figs. 11–13 are plotted a representative sample of the proton-nucleus spin analyzing power (polarization) observables using the same legend as in all earlier figures. In Fig. 11 which examines tradition nuclear targets, all the calculations do well. The fitting of the polarization variable simultaneously with the differential cross section involved an interesting tension between the relative weight of the χ^2 of both observables since the polarization is normalized by the differential cross section. The results show that in many instances this work (the WP OMP) fit the polarization better than it did with the differential cross section. In all three polarization figures the major difficulty was again with the lighter nuclei, specifically the carbon isotopes [49,117] as depicted in Figs. 12 and 13.

The global optical potential of this work is the best in reproducing this spin observable over a wide range of targets and chains of nuclei. Additional polarization experimental data are always welcome because they measure the interference between the central and spin-orbit terms and therefore is a good constraint on their relative strengths. The present data set has a satisfactory amount of these reactions at projectile energies lower than 100 MeV but additional higher energy polarization experiments would be appreciated.

C. Isoscalar strength

To analyze optical potentials it has often been instructive to calculate the volume integrals of the various terms to further illicit theoretical comparison. In Fig. 14 the central real and imaginary isoscalar volume integral components at 50 MeV and 150 MeV projectile energy are reproduced. There is some ambiguity in determining the isoscalar component for the OMPs discussed here so the technique used was the average between the proton-nucleus and the neutron-nucleus central volume integrals. Using this definition the central potential of all traditional OMPs can be split into the isoscalar and isovector integrals, respectively,

$$\mathcal{V}_V(E) = V_0(E) + \mathcal{I}(E), \tag{28}$$

where $\mathcal{I}(E)$, the isovector component, has its sign dependent on the isospin projection of the projectile and $V_0(E)$ is the isoscalar term. For Fig. 14 a representative sample of nuclei was chosen that is on or near the line of stability, the explicit list of nuclei used in the calculations is listed in the figure caption. The green, red, and blue lines are the WP, KD, and MD OMPs volume integrals of the isoscalar term ($V_0(E)$), respectively, and they have broad agreement which is encouraging. All three potentials, fit independently to experimental data, developed roughly the same strength for the isoscalar central component. The only large discrepancy is the MD OMP at low energy has a much smaller imaginary component because it is missing a surface term. The other two OMPs at this energy (KD and WP) have a significant imaginary surface term which adds to the strength of the attractive central potential. Incidentally if the WP OMP of this work is examined closely in Fig. 14 protrusions are seen, especially in the imaginary panels. These are due to the new magic number term that the potential has included [Eqs. (7), (10)]. The ramifications of this inclusion are not readily apparent in comparisons with the reaction data, future studies on the effect of closed shells on optical potential behavior would be fruitful.

To elicit further insight the volume integrals created from microscopic Watson $t - \rho$ (nucleon-nucleon scattering matrix folded with target density) potentials [118–120] are plotted in light gray in Fig. 14. The specific apparatus was developed, in part, by the earlier work of one of the present authors (S.P.W.) and detailed in Refs. [121–123]. In brief, the light gray shaded regions use a variety of nucleon-nucleon potentials [124–126] folded with theoretical densities [127,128] using a variety of techniques. These microscopic optical potentials have been satisfactory in reproducing experiment at the lower energies and better at the higher energies. Rarely do the microscopic potentials, which have different fundamental motivations, match the quality of these three phenomenological potentials in reproducing these observables. Significant systematic differences are recognized in the isoscalar volume integrals

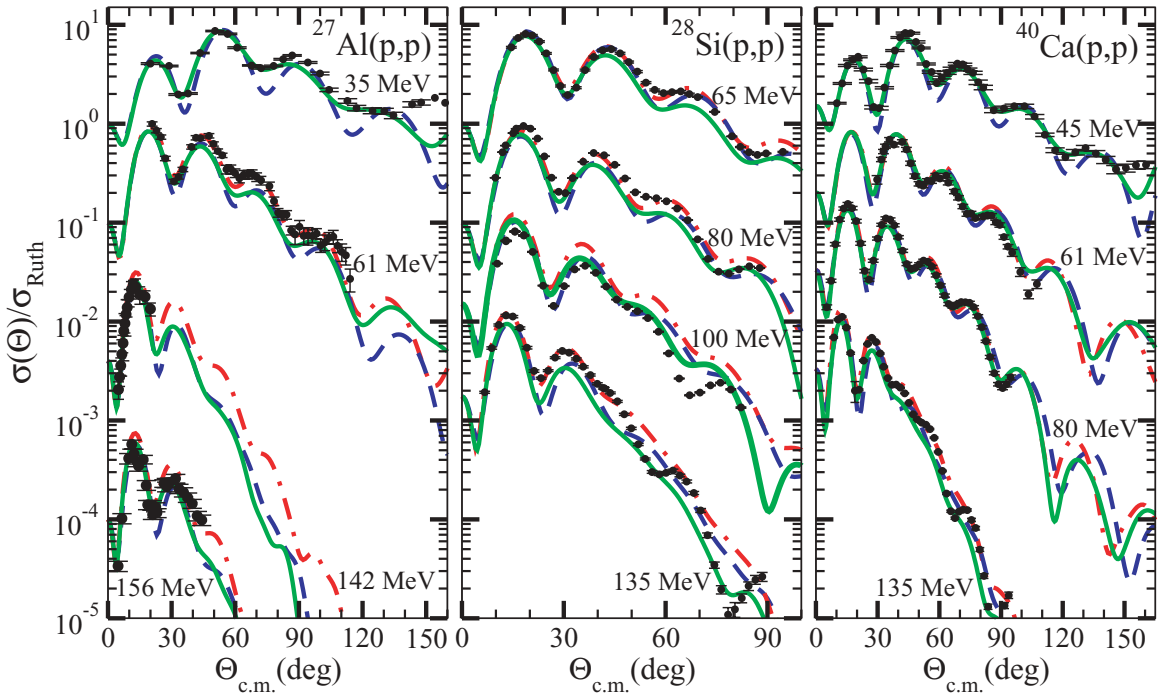

FIG. 7. (Color online) Proton-nucleus elastic Rutherford reduced differential cross section experimental data for the target nuclei of ^{27}Al [37,38,58,104,105], ^{28}Si [42,106], ^{40}Ca [5,38,70], at varying proton laboratory energies. Refer to Fig. 5 for details of the legend for the theoretical calculations.

especially in the light nuclei and the imaginary term but there are also regions of general agreement.

In summary, these three OMPs describe the known elastic scattering data well and have similar isoscalar magnitudes.

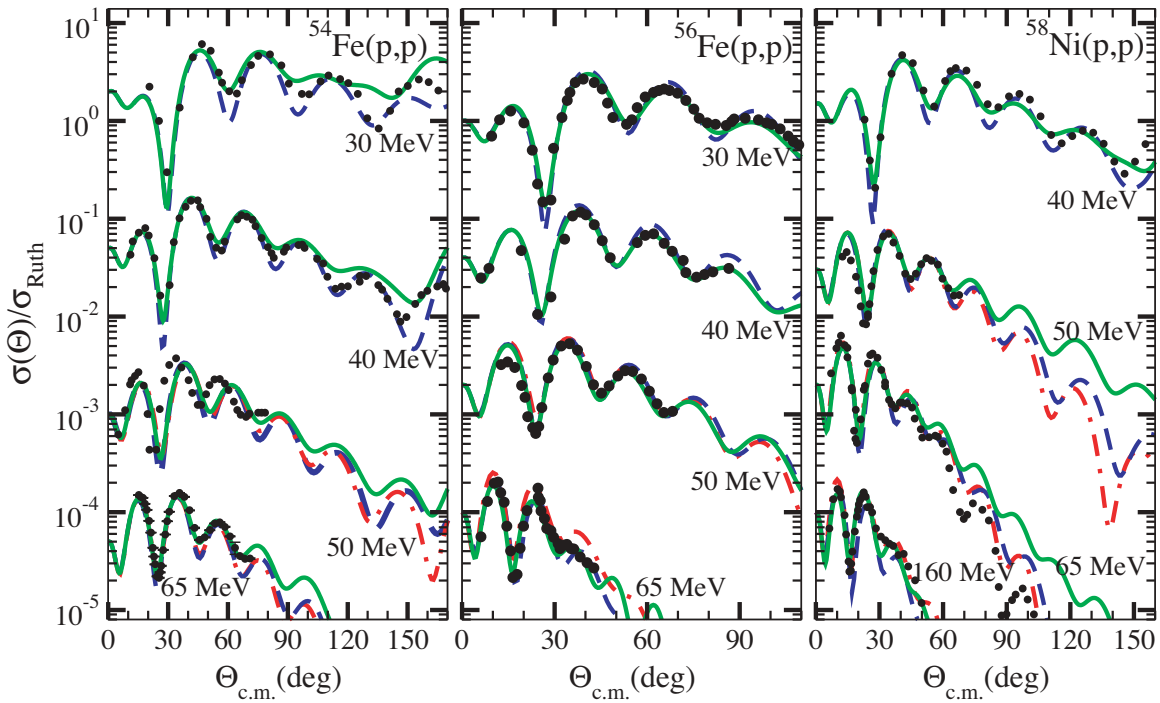

FIG. 8. (Color online) Proton-nucleus elastic Rutherford reduced differential cross section experimental data for the target nuclei of ^{54}Fe [21,72,74,81], ^{56}Fe [8,72,82,84], ^{58}Ni [84,107–109], at varying proton laboratory energies. Refer to Fig. 5 for details of the legend for the theoretical calculations.

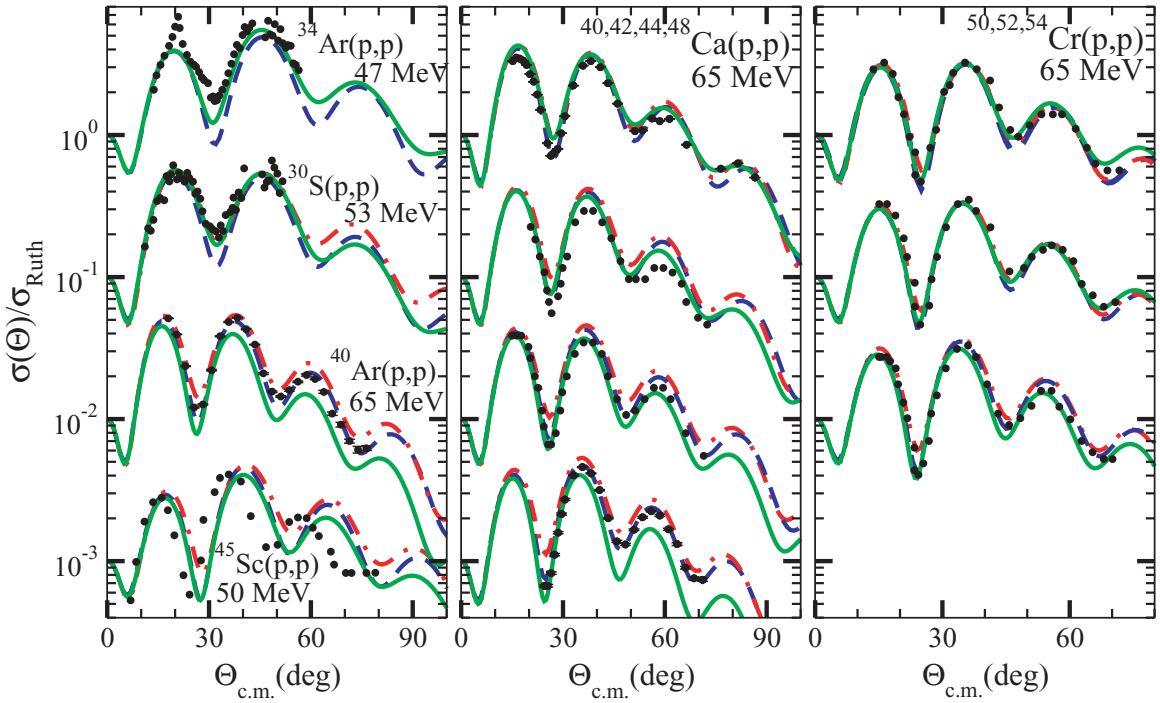

FIG. 9. (Color online) Proton-nucleus elastic Rutherford reduced differential cross section experimental data for the target nuclei of ^{34}Ar [66,110], ^{30}S [110], ^{40}Ar [74], ^{45}Sr [72], ^{40,42,44,48}Ca [71,74], ^{50,52,54}Cr [71], at varying proton laboratory energies. The target labels at the top read left to right correspond to the calculations and experimental data read top to bottom for the two rightmost panels. Refer to Fig. 5 for details of the legend for the theoretical calculations.

Detailing their advantages; the KD OMP is well suited for neutron projectile projects, the MD OMP, in its simplicity, does well with differential cross sections, and the WP OMP has strengths in the exotic nuclei and in the spin observables.

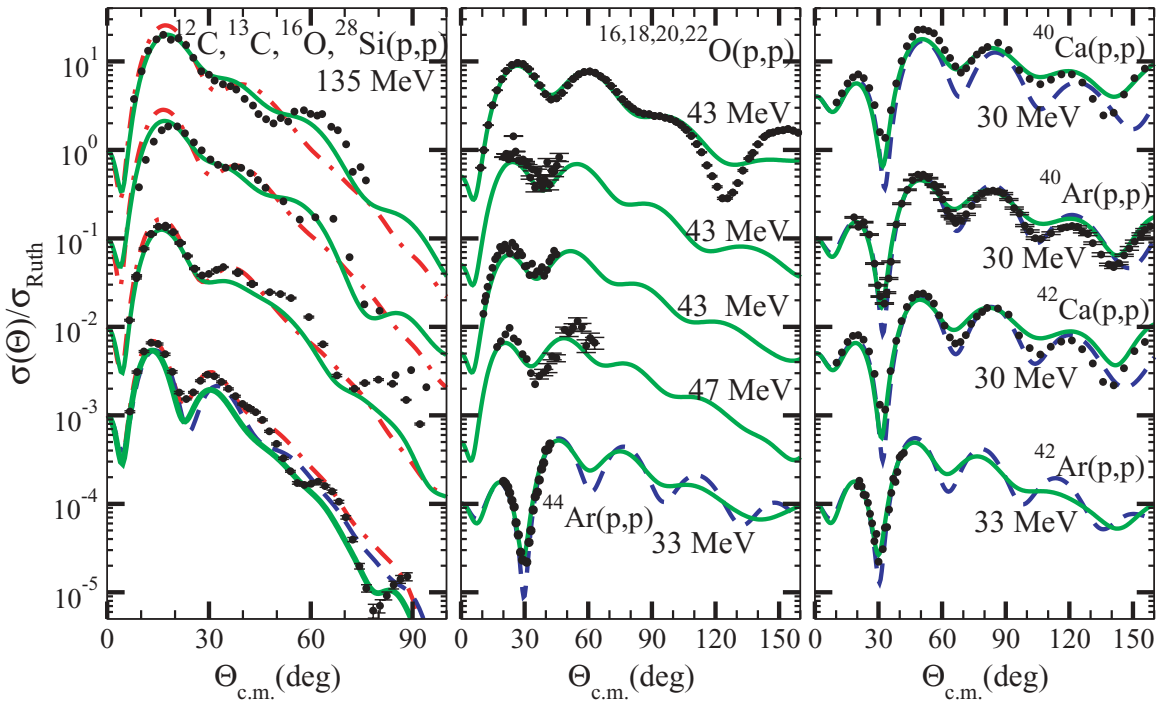

FIG. 10. (Color online) Proton-nucleus elastic Rutherford reduced differential cross section experimental data for the target nuclei of ^{12,13}C [36,51], ^{16}O [48,56], ^{18,20,22}O [50,57,110], ^{28}Si [106], ^{40,42}Ca [70,82], ^{40,42,44}Ar [68,69], at varying proton laboratory energies. The target labels at the top read left to right correspond to the calculations and experimental data read top to bottom for the two leftmost panels. Refer to Fig. 5 for details of the legend for the theoretical calculations.

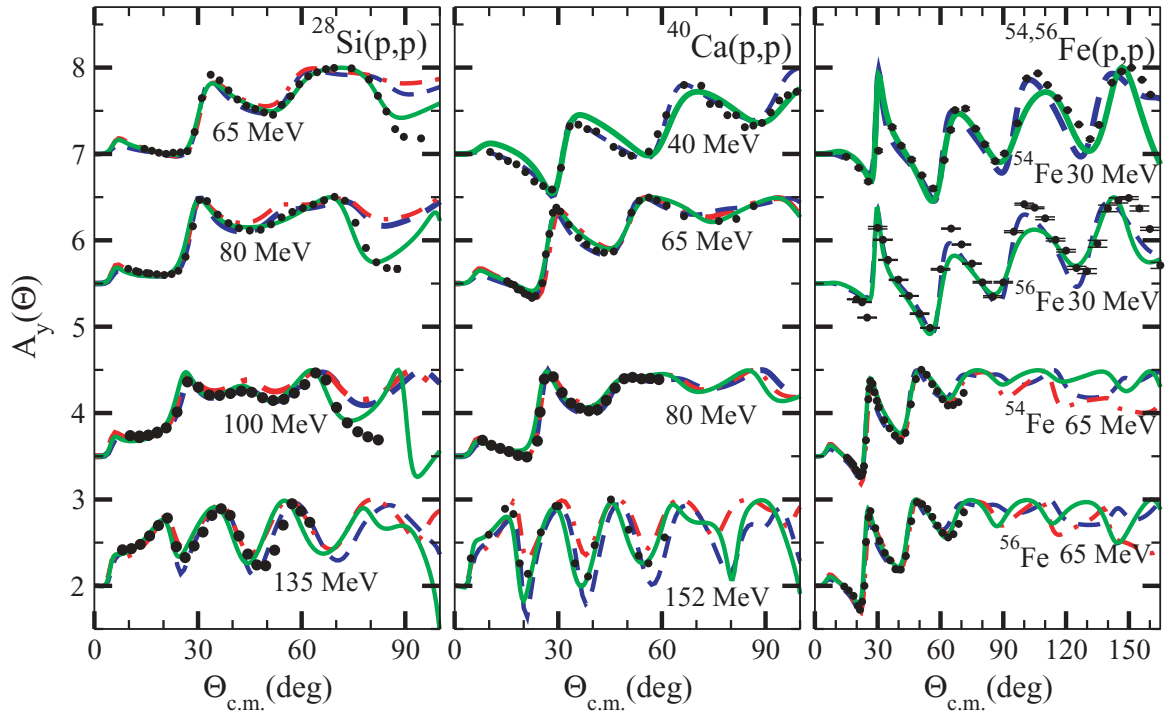

FIG. 11. (Color online) Proton-nucleus elastic analyzing power spin observable experimental data for the target nuclei of ^{28}Si [74,106], ^{40}Ca [43,74,113,114], ^{54,56}Fe [21,74,84,115], at varying proton laboratory energies. Refer to Fig. 5 for details of the theoretical calculations.

In the next section larger theoretical differences will be proffered, while examining the isovector components, that will eventually lead to quite disparate scattering observable results.

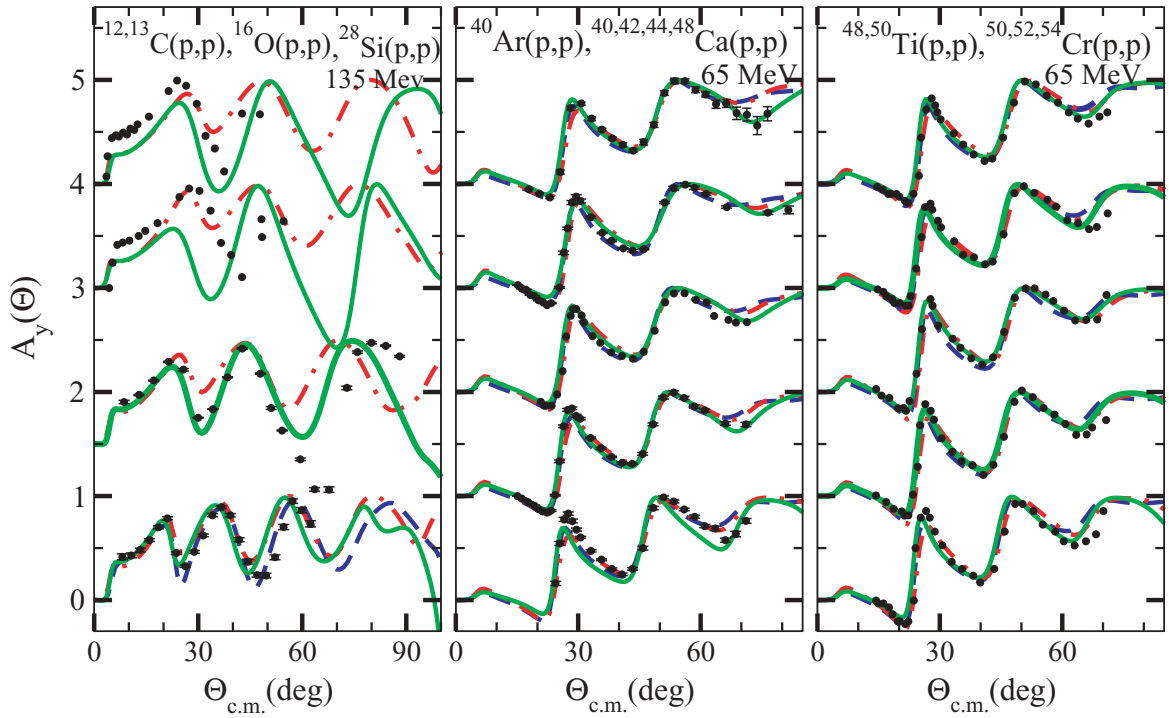

FIG. 12. (Color online) Proton-nucleus elastic analyzing power spin observable experimental data for the target nuclei of ^{12,13}C [36,51], ^{16}O [56], ^{28}Si [106], ^{40,42,44,48}Ca [73,74], ^{40}Ar [52], ^{48,50}Ti [52], ^{50,52,54}Cr [73], at varying proton laboratory energies. The target labels at the top read left to right correspond to the calculations and experimental data read top to bottom. Refer to Fig. 5 for details of the theoretical calculations.

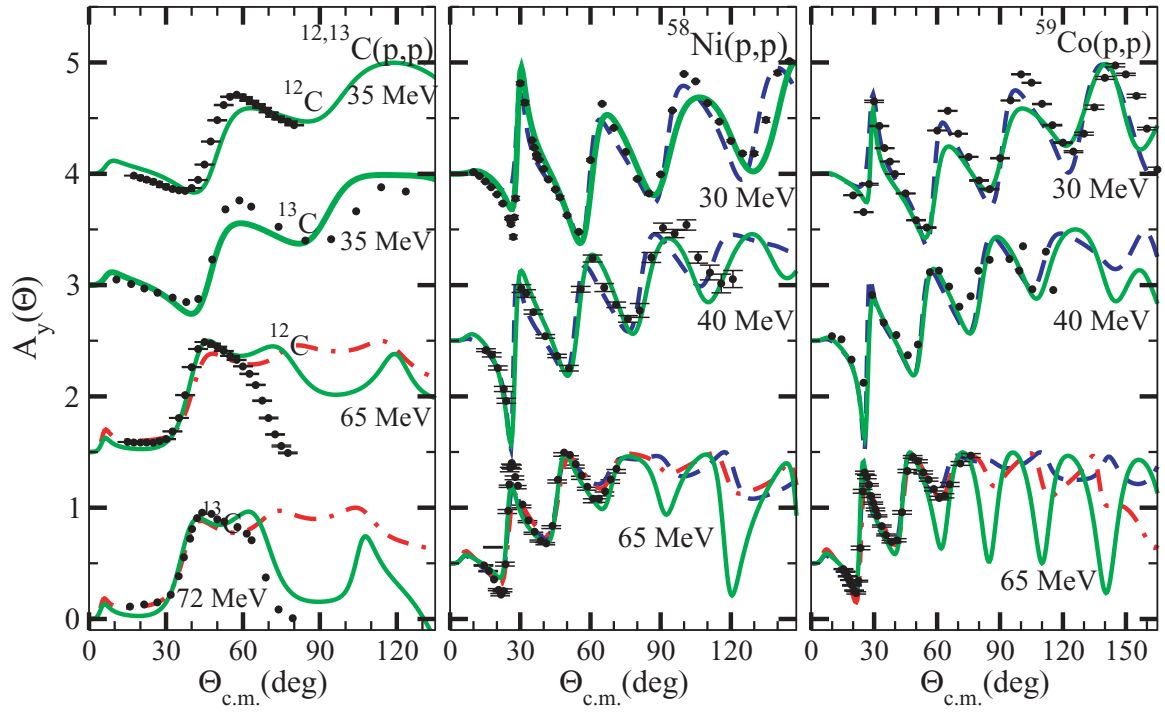

FIG. 13. (Color online) Proton-nucleus elastic analyzing power spin observable experimental data for the target nuclei of ^{12,13}C [20,20,25,30], ^{58}Ni [84,107,116], ^{59}Co [83,84,115], at varying proton laboratory energies. Refer to Fig. 5 for details of the theoretical calculations.

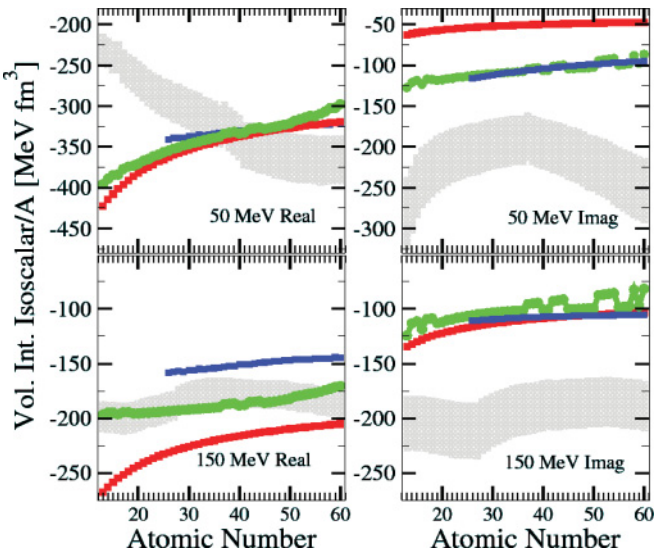

FIG. 14. (Color online) A figure of theoretical comparisons. Plotted are the isoscalar volume real and imaginary space integrals between the three potentials that are under examination at 50 MeV and 150 MeV projectile energy. The light green, medium blue, and dark red lines represent the WP, KD, and MD OMPs respectively. The light gray shaded area represents typical volume integrals for microscopic $t-\rho$ potentials (as detailed in the text). Each atomic number has a sample nuclei attache to it. These nuclei are: ^{13}C, ^{14}C, ^{15}N, ^{16}N, ^{17}O, ^{18}O, ^{19}F, ^{20}F, ^{21}Ne, ^{22}Ne, ^{23}Na, ^{24}Na, ^{25}Mg, ^{26}Mg, ^{27}Al, ^{28}Al, ^{29}Si, ^{30}Si, ^{31}P, ^{32}P, ^{33}S, ^{34}S, ^{35}Cl, ^{36}Cl, ^{37}Cl, ^{38}Ar, ^{39}K, ^{40}Ar, ^{41}K, ^{42}Ca, ^{43}Ca, ^{44}Ca, ^{45}Sc, ^{46}Ti, ^{47}Ti, ^{48}Ti, ^{49}Ti, ^{50}V, ^{51}V, ^{52}Cr, ^{53}Mn, ^{54}Fe, ^{55}Mn, ^{56}Fe, ^{57}Co, ^{58}Ni, ^{59}Co, ^{60}Ni. These same nuclei will be used in many of the remaining figures.

V. ISOVECTOR TERM ANALYSIS

The asymmetry isovector term, which measures target neutron and proton imbalance, is a point of illustrative comparison and will be the focus of this section. This research attempted to develop an isospin consistent potential solely by fitting to elastic experimental reaction data, here the success of this effort will be assessed. First the historical ansatz of a simple linear $N-Z$ dependence for this potential term will be examined, then a Lane analysis check of the isospin character of this OMP will be proffered. Finally a detailed comparison of the isovector volume integral of the three OMPs alongside microscopic optical potential results will occur with connections to experiment established.

A. Validity of $N-Z$

Recently the simple linear $N-Z$ dependence of the asymmetric potential has been called to question [9]. All three phenomenological potentials, following tradition, have used this standard so it is informative to use microscopic techniques to develop the optical potential from the nucleon-nucleon potential to gain insight into the origin of this $N-Z$ term (following Refs. [129–131]). The potential between two nucleons usually contains isospin vector components (usually a spin dependent and a spin independent piece, for simplification here they are combined). Assuming the valid impulse approximation at high energies, the techniques of Kerman, McManus, and Thaler [132] and Watson [118,119,121,122] can be used to construct the nucleon-nucleus optical potential

from a sum of nucleon-nucleon potentials:

$$V_{\text{asym}} \approx \sum_{i}^{A} V_{\text{iso}\,NN}(\tau_{\text{proj}} \cdot \tau_i), \tag{29}$$

switching over to raising and lowering operators

$$V_{\text{asym}} \approx \sum_{i}^{A} V_{\text{iso}\,NN} \frac{1}{2}(\tau_{\text{proj}_+}\tau_{i_-} + \tau_{\text{proj}_-}\tau_{i_+} + 2\tau_{\text{proj}_z}\tau_{i_z}). \tag{30}$$

If the difference of the asymmetry piece between the proton projectile and neutron projectile on the same target is calculated then microscopically it has this format:

$$\begin{aligned} &V_{\text{asym}}\left(t_{\text{proj}} = +\frac{1}{2}\right) - V_{\text{asym}}\left(t_{\text{proj}} = -\frac{1}{2}\right) \\ &\approx V_{\text{iso}\,NN}\left(\frac{N}{2}\tau_{\text{proj}_-} - \frac{Z}{2}\tau_{\text{proj}_+}\right) \\ &\quad - V_{\text{iso}\,NN}\left(\frac{N-Z}{4}\left(\tau_{\text{proj}_z}\left(+\frac{1}{2}\right) + \tau_{\text{proj}_z}\left(-\frac{1}{2}\right)\right)\right). \end{aligned} \tag{31}$$

The first two terms are the simplest inelastic charge-exchange terms, often referred to as quasi-elastic charge-exchange [130] because they do not involve the direct exchange of nucleons and they are between isobaric analog states. The first inelastic term is exclusively nonzero for the proton projectile, the second inelastic term is nonzero exclusively for the neutron projectile and the last two terms are the elastic contributions (the same contribution occurs for both the proton or neutron projectile). A direct $N - Z$ factor is derived directly from the elastic scattering component, the inelastic term does not contain the equivalent proportionality (the proton potential contains a nonzero N and the neutron potential contains a nonzero negative Z however these potentials are not implemented simultaneously). This is the first affirmation that a linear $N - Z$ term in the optical potential, which by definition is both refractive (elastic) and absorptive (inelastic), is to first order valid but somewhat simplistic. The imbalance of neutrons to protons does control the physical mechanisms of the elastic isovector piece whereas the number of absolute neutrons (for proton scattering) or the number of absolute protons (for neutron scattering) are the source of strength for the inelastic component. Although this type of impulse microscopic approximation does not intrinsically contain multiple scattering, correlations, exchange, or coupled channels, it is a good approximation at higher energies (it has been shown to work adequately at projectile energies of 150 MeV [120]) and it signifies that beyond first order the asymmetry term needs a theoretical re-evaluation.

Writing the asymmetric potential in macroscopic nucleon-nucleus optical potential form is also illuminating:

$$\begin{aligned} V_{\text{asym}} &= V_{\text{iso}\,NA}(\tau_{\text{proj}} \cdot \tau_{\text{targ}}) \\ &= V_{\text{iso}\,NA}(\tau_{\text{proj}_+}\tau_{\text{targ}_-} + \tau_{\text{proj}_-}\tau_{\text{targ}_+} + \tau_{\text{proj}_z}\tau_{\text{targ}_z}), \end{aligned} \tag{32}$$

and likewise the difference equation subtracting neutron scattering from proton scattering is

$$\begin{aligned} &V_{\text{asym}}\left(t_{\text{proj}} = +\tfrac{1}{2}\right) - V_{\text{asym}}\left(t_{\text{proj}} = -\tfrac{1}{2}\right) \\ &\quad \approx V_{\text{iso}\,NA}(\tau_{\text{proj}_-}\tau_{\text{targ}_+} - \tau_{\text{proj}_+}\tau_{\text{targ}_-} + \tau_{\text{targ}_z}). \end{aligned} \tag{33}$$

This form again demonstrates a direct connection to both elastic scattering and inelastic charge-exchange. The elastic z component piece is proportional to $\tau_{\text{targ}_z} = N - Z$, which confirms the earlier microscopic results. Similarly the inelastic piece is again ambiguous. In many nuclei the ground state has an isospin vector designation such that τ_{targ_z} is the maximum value and thus $|\tau_{\text{targ}_-}| = |\tau_{\text{targ}_+}| \propto \sqrt{N - Z}$ but with unstable deformed nuclei this is not always the case [133] and therefore a general rule about the strength of the inelastic piece should be treated with apprehension, especially at higher energy [130, 134]. Both the microscopic and macroscopic formulations of the optical potential lead to a differentiation between the elastic and inelastic charge-exchange component's constant of proportionality as seen in previous work [129–131,134–136].

All the global optical potentials, perhaps because of the linear $N - Z$ term, have trouble giving excellent results for the calcium and chromium isotopes (Figs. 9 and 10). Similarly, as exploration further from the line of stability occurs, it is realized that using a stark absolute linear term leads to erroneous results. For example using a 100 MeV neutron projectile gives physical results when scattering from ^{12,13,14,15}C using the WP OMP but it begins to give negative total cross sections for the same scattering observables if the target is ^{16}C. Obviously all elements will return nonphysical results when the asymmetric term allows for unimpeded linear growth as the neutron-proton imbalance gets larger (especially if this term is large as is the case for carbon for the WP OMP). In general the linear $N - Z$ structure is a good first approximation but a better formulation should be developed for exotic nuclei optical potentials far from the line of stability.

B. Lane analysis

A Lane consistent potential [3,129,134–137] guarantees a near equivalent isoscalar and isovector nuclear potential for proton and neutron projectiles at the same initial projectile bombarding energies and thus the measure of Lane consistency is a good check on the integrity of the isovector term.

As discussed in Sec. IV C, the volume potential of all traditional OMPs can be split into the isoscalar and isovector parts, respectively,

$$\mathcal{V}_V(E) = V_0(E) + \mathcal{I}(E), \tag{34}$$

where $\mathcal{I}(E)$, the isovector component, has its sign dependent on the isospin projection of the projectile. Because the effective short range projectile kinetic energy of the proton-nucleus potential is different than in the corresponding neutron-nucleus potential, a Lane consistent potential will add a Coulomb correction term, Δ_c to the traditional proton-nucleus OMP,

$$\mathcal{V}_V(E) = V_0(E) + \mathcal{I}(E) + \Delta_c, \tag{35}$$

which adjusts the energy dependent proton-nucleus potential to account for the lessening of the initial bombarding energy of the charged projectile as it heads toward the target due to

the long range Coulomb field [129]. To be all inclusive this correction should be included for the complex volume and spin orbit pieces, traditionally however it has only been applied to the real central term (recent exceptions are Refs. [9,134]).

Using the notation of Eqs. (5)–(27) of this WP potential the real central Coulomb correction, Δ_c, can easily be derived as

$$\mathcal{V}_V(E)+\mathcal{V}_S(E)=\mathcal{V}_V(E-f_{\rm coul})+\mathcal{V}_S(E,-f_{\rm coul})+\Delta_c(E), \tag{36}$$

where E is the original projectile bombarding energy and the volume, surface, and Coulomb potentials are defined using Eqs. (3)–(4), (5)–(7), (11). This equation leads directly to a solution as

$$\Delta_c=\mathcal{V}_V(E)+\mathcal{V}_S(E)-\mathcal{V}_V(E-f_{\rm coul})-\mathcal{V}_S(E-f_{\rm coul}), \tag{37}$$

which is effectively the difference between the original and an energy adjusted central volume term. All three of the OMPs examined contain a Coulomb correction term.

Equation (37) represents the exact definition of the real Coulomb correction. Historically, starting with Ref. [3], an ansatz was made to use a Woods-Saxon potential form with the strength proportional to the average Coulomb potential in the short range to approximate this Coulomb correction, both the KD and MD OMP take this approach. The WP OMP uses a different approximate form, instead of attaching the Coulomb correction term to the volume term (with Woods-Saxon shape) it is combined with the Coulomb term by having the radius of the short term Coulomb potential, Eq. (26), becomes artificially larger and uncharacteristically energy and atomic number dependent. The Coulomb correction of this work is defined as

$$\Delta_c\approx(f_{\rm coul}(\mathcal{R}_C)-f_{\rm coul}(\mathcal{R}_{C_0}=1.20\times A^{\frac{1}{3}}\,{\rm fm})), \tag{38}$$

in which a literal addition to the Coulomb potential was devised by extending $\mathcal{R}_C$ beyond its traditional value. To extract this Coulomb correction to the nuclear term we subtracted the known short ranged Coulomb potential from the full-extended fitted Coulomb potential of this work as Eq. (38) details.

This nontraditional approach has some advantages. First it disentangles the unknown Coulomb correction from the likewise unknown nuclear volume term and combines it to the more apparent short range Coulomb force. Second, as developed in Ref. [137], a Woods-Saxon shape is not an excellent functional representation of the exact Coulomb correction result (see Fig. 11 of Ref. [137] for example). The approximate Coulomb correction of this work [Eq. (38)] more satisfactorily represents the shape of the exact result. Giving an example, in Fig. 15 are depicted two examples at the commonly tested experimental projectile energy of 65 MeV. The black line represents the calculation of the exact result, the green line is the function which this research developed in the process of fitting the Coulomb radius to the global data set using Eq. (38). The thin dashed red line is the Woods-Saxon shape normalized to this approximation added as a reference. Although the green fit of this research does not always match the exact result, its functional shape is closer to the exact result specially in the important interior region. Another reason to use this approximation is that this correction has an operational advantage that it can be easy be added to modern optical codes like ECIS [15] by changing the value of the Coulomb radius. The exact result of Eq. (37), which does not have a closed analytical form, cannot be added neatly.

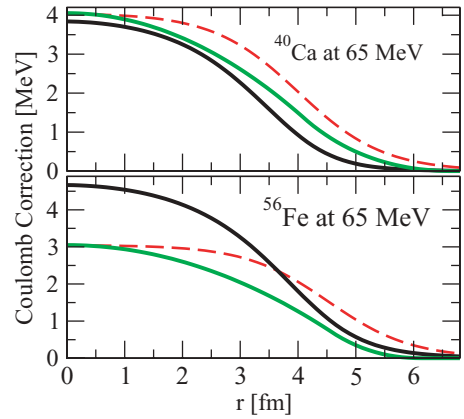

FIG. 15. (Color online) These are two example depictions at 65 MeV projectile energy of the functional coulomb correction potential for the targets ^{40}Ca and ^{56}Fe respectively. The solid black line is the magnitude of the exact calculation (the coulomb correction is actually negative), for the potential of this work, using Eq. (37). If the coulomb correction term is applied to the proton-nucleus optical potential then the potential can be considered isovector Lane consistent (described in the text). The solid green line is the approximate function which was determined in this work by fitting the global nucleon-nucleus data sets. This approximate form was determined by Eq. (38). The thinner red dashed line is given as an example Woods-Saxon functional form for comparison.

To examine if this inclusion of a Coulomb correction term brings the WP OMP closer to Lane consistency the contour graphs of Figs. 16 and 17 are introduced. They map over the complete applicable projectile energy and atomic number of target phase space for the WP OMP and the measure of Lane inconsistency is normalized to the moduli of the central potential. The figures have ranges between 4% and 10% Lane inconsistency. It is noted that of reactions in this phase space the real central Coulomb correction is at worst about a 12% correction. Figure 16, top panel, shows the level of inconsistency without a Coulomb correction (with an average inconsistency of 4.3%). The systematic need for a Coulomb correction for the present potential is apparent especially at lower energies and larger targets, these sensitivities are congruent with the Coulomb correction term developed in the KD OMP of Ref. [1] which increases linearly with Z and to good approximation decreases linearly with E.

The real central Coulomb correction is inherently included in this potential, as discussed above, and with it the WP potential is substantially more Lane consistent as depicted in Fig. 16, bottom panel. Much more of the phase space is now below the 4% level and only in a few small regions does the Coulomb correction addition make the potential less Lane consistent (high A and high E and low A at midrange energies). The areas where the Coulomb correction was substandard is where the experimental data are sparse, especially lacking neutron reactions. For example, two experimentally popular projectile bombarding energies are at 65 MeV and 135 MeV.

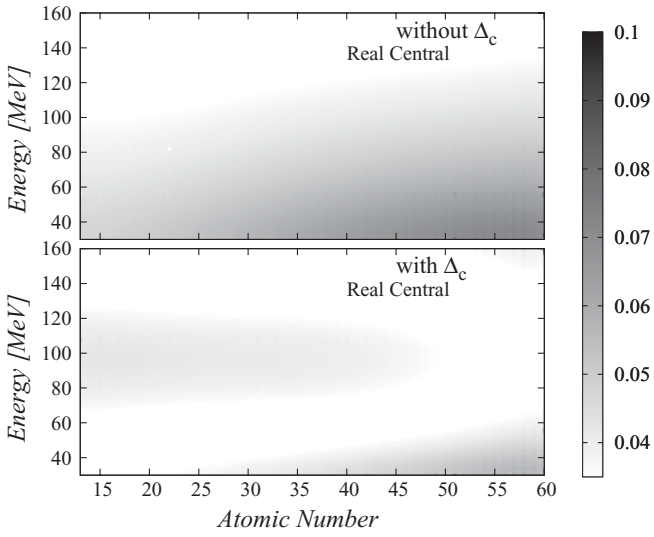

FIG. 16. This is a depiction in projectile energy-target atomic number phase space of the **real** fraction Lane inconsistency relative to the magnitude of the total moduli of the central potential for sample nuclei. The top panel shows the optical potential of this work **without** a coulomb correction term assuming only $\mathcal{R}_c = 1.20 \times A^{\frac{1}{3}}$ fm. The bottom panel depicts the same but **with** a coulomb correction term assuming a dynamic E and A dependent coulomb radius, $\mathcal{R}$, described in the text. The unweighted average for the whole phase space of the top panel is 0.043 Lane inconsistency. The unweighted average for the whole phase space of the bottom panel is 0.034 Lane inconsistency. The fraction of 0.04 is assumed here to be a pragmatic minimum and a measure of sufficient Lane isovector consistency. The sample nuclei for each atomic number were near or on the line of stability and are the same as those in Fig. 14.

Here, with the Coulomb correction included (as shown in the bottom panel of Fig. 16), the Lane consistency is very good. The energies between these guideposts are where the fit has difficulties. The average value of Lane consistency with the Coulomb correction is 3.4%. In our studies developing this analysis it was found that using a constant energy independent $\mathcal{R}_c$ between $(1.1 \times A^{\frac{1}{3}})$ fm and $(1.35 \times A^{\frac{1}{3}})$ fm to represent

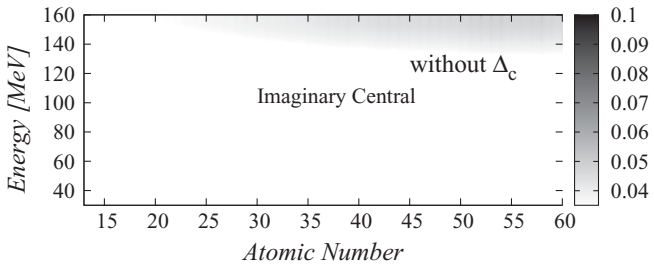

FIG. 17. This is a depiction in projectile energy-target atomic number phase space of the **imaginary** fraction Lane inconsistency relative to the magnitude of the total complex central force for sample nuclei which are listed in Fig. 14. Overall the isospin inconsistencies are smaller than its real counterpart until $E > 140$ MeV. The unweighted average for the whole phase space is 0.025 Lane inconsistency. The fraction of 0.04 is assumed here to be a pragmatic minimum and a measure of sufficient Lane isovector consistency.

the fixed traditional short range Coulomb radius in Eq. (38) produced the best results which is reassuring because it matches the standard short range Coulomb potential found in the literature.

The imaginary Coulomb correction term has been ignored in the KD, MD, and this potential. It has been argued that it can be neglected because it is small [136,138] or because of lack of sufficient experimental data it will be ambiguous [1]. In performing this analysis we found it to be small at low energy but unfortunately at high energy (greater than 120 MeV projectile energy) it begins to be significant in contrast with the real Coulomb correction term which diminishes as depicted in Fig. 17. The average of the Lane inconsistency over the entire phase space normalized to the magnitude of the complex WP central potential measures 3.4% in the real term and 2.5% for the imaginary term. However the imaginary Lane inconsistency can run higher than 9% for $A > 60$ and $E > 160$ MeV.

Examining the quality of the results in reproducing experimental reactions in Sec. IV there is significant error in the neutron total cross section calculation at high atomic number and high energy as represented in Fig. 4. Since this potential fits the proton and neutron observables simultaneously this could be due to the lack of that imaginary Coulomb correction term. In future high energy optical potential work this imaginary correction should not be neglected.

The requirement that the optical potential of this work be completely Lane consistent is not congruent with the goals of this research or the general character of the nuclear force. Charge-dependent (isospin symmetry breaking) discoveries [139,140], the uncertainty in the short range Coulomb potential, and the approximate functional forms applied in the phenomenological optical potentials all diminish the importance of attaining perfect isospin nuclear symmetry and a Lane potential. The goal of under 4% inconsistency seems to be a reasonable pragmatic minimum giving these conditions. This research aimed to be as pure a phenomenological fit as possible letting the reproduction of experimental data confirm what microscopic theory has shown elsewhere regarding the Coulomb correction [134,137,141]. The conclusion is that there is good agreement when there is a copious amount of experimental data giving credence to the technique employed.

C. A comparison

A comparison of the three global optical potentials isovector asymmetry terms, which use the traditional $N - Z$ terms, now follows. Here dramatic differences between the three formulations can be isolated.

Starting from the simplest potential, the MD OMP has a neutron excess asymmetric term for the real volume and the real spin-orbit amplitude only [2]:

$$\mathcal{I}_{MD} = \pm\frac{N-Z}{A}16.5 f_{WS}(r, \mathcal{R}_i, \mathcal{A}_i) \mp \frac{N-Z}{A}3.75\frac{d}{dr} f_{WS}(r, \mathcal{R}_{SO}, \mathcal{A}_{SO})(\mathbf{l}\cdot\sigma), \quad (39)$$

which has no explicit energy dependence and has the standard linear term of $\frac{N-Z}{A}$. The difference between the proton projectile and the neutron projectile is simply a sign change, the internal geometry parameters have no isospin dependence.

The KD OMP has an explicit asymmetry term only for the real volume component and the imaginary surface component [1]

$$\begin{aligned}\mathcal{I}_{KD} = &\pm\frac{N-Z}{A}\big(21.0(1-v_2(E-E_f)+v_3(E-E_f)^2\\ &-7.0\times10^{-9}(E-E_f)^3)f_{WS}(r,\mathcal{R}_{iv},\mathcal{A}_{iv})\big)\\ &\mp i4\mathcal{A}_d\,\frac{N-Z}{A}\left(16\frac{(E-E_f)^2}{(E-E_f)^2+{d_3}^2}\right.\\ &\left.\times\exp(-d_2(E-E_f))\frac{d}{dr}(f_{WS}(r,\mathcal{R}_d,\mathcal{A}_d)\right),\end{aligned}\tag{40}$$

where v_2, v_3, d_2, and d_3 are functions which depend on the nucleon number of the target, and projectile energy and the isospin character of the projectile. Likewise E_f represents the Fermi energy of the target, extracted from mass excess values [142], and is dependent on the isospin projection of the projectile. The internal geometry parameters have no explicit isospin dependence. Because of the separate functional dependence on the projectile the asymmetry term, I_{KD} of Eq. (40), is not exactly linear and the isospin flip in the projectile is not simply a sign change as with the I_{MD} term given by Eq. (39).

The optical potential of this work (WP OMP), outlined in Sec. II A, has vector isospin asymmetry $(N-Z)$ in five major terms: real and imaginary volume, imaginary surface, and real and imaginary spin orbit [Eqs. (6), (9), (13), (15), (17)]:

$$\begin{aligned}\mathcal{I}_{WP} = &\pm(N-Z)(V_{V_i}+iW_{V_i})f_{WS}(r,\mathcal{R}_i,\mathcal{A}_i)\\ &\mp i4(N-Z)\mathcal{A}_S W_{S_i}\frac{d}{dr}f_{WS}(r,\mathcal{R}_S,\mathcal{A}_S)\\ &\mp(N-Z)(V_{SO_i}+iW_{SO_i})\frac{d}{dr}f_{WS}(r,\mathcal{R}_{SO},\mathcal{A}_{SO}),\end{aligned}\tag{41}$$

where V_{V_i}, W_{V_i}, W_{S_i}, V_{SO_i}, and W_{SO_i} are separable polynomial functions in terms of projectile energy and nucleon number [Eqs. (5)–(27)]. There is no projectile isospin dependence within the polynomials. This potential also enforces the separability of E and A by using $(N-Z)$ and not $\frac{N-Z}{A}$. There are some explicit asymmetry terms in the $\mathcal{A}_V$ [Eq. (20)] and $\mathcal{R}_{SO}$ [Eq. (24)] geometry terms which also lead to nonsymmetric neutron excess terms. This optical potential has therefore attempted to fit the imaginary volume, surface, and spin orbit asymmetry terms, the other contemporary global OMPs discussed within have set their explicit imaginary asymmetric terms to zero.

To explore the differences between the three OMPs further let us again examine volume integrals which have been illustrative in the past to help describe Gamow-Teller and Fermi charge-exchange transitions [143] and to effectively compare the strength of disparate shaped optical potentials. Explicitly calculated are, using the notation of Eq. (2), the following integrals:

$$\begin{aligned}J_{V_V}/A = &-\frac{4\pi}{A}\int_0^\infty r^2(\mathcal{V}_V(E,A,N,Z,\mathcal{P},MN))\\ &\times f_{WS}(r,\mathcal{R}_V,\mathcal{A}_V)\,dr,\end{aligned}\tag{42}$$

$$\begin{aligned}J_{W_V}/A = &-\frac{4\pi}{A}\int_0^\infty r^2(\mathcal{W}_V(E,A,N,Z,\mathcal{P},MN))\\ &\times f_{WS}(r,\mathcal{R}_V,\mathcal{A}_V)\,dr,\end{aligned}\tag{43}$$

$$\begin{aligned}J_{W_S}/A = &+\frac{4\pi}{A}4\mathcal{A}_S\int_0^\infty r^2(\mathcal{W}_D(E,A,N,Z,\mathcal{P}))\\ &\times\frac{d}{dr}f_{WS}(r,\mathcal{R}_S,\mathcal{A}_S)\,dr.\end{aligned}\tag{44}$$

These equations will be used to calculate the differences in volume integrals between a proton projectile and a neutron projectile acting upon the same target nucleus (the isospin asymmetry). The difference is emphasized, as it was in the linear study of the $N-Z$ term, because this is what characterizes the isovector asymmetry term from the rest of the dominating isoscalar nuclear potential; it does not disappear upon subtraction of this isospin flip of the projectile. In the KD potential, where there are two separate potentials with different functions to differentiate proton and neutron scattering, this definition of asymmetry is somewhat ambiguous, it is much more enhanced than simply the $N-Z$ term. So in this comparison we will define isovector to be half the difference between the proton-nucleus and neutron-nucleus potential. This will include the addition of the nuclear Coulomb correction term in the proton potential for all three of the OMPs. This seems to be the best workable definition for isovector for these three potentials especially in tandem comparisons with the microscopic potential that follow.

In Fig. 18 the two panels contain results of the real volume, surface, and Coulomb correction integral difference at 50 MeV (left panel) and 150 MeV (right panel) energy between a proton and a neutron projectile for the three global optical potentials (approximately twice the isovector strength). This volume integral difference is a direct measure of the change in strength that the three potentials have for the dynamics of a isospin flip of the projectile on the same $N-Z\neq0$ target. For every nucleon number ($13\leqslant A\leqslant 60$) there was chosen a representative target that is stable or close to the line of stability which are listed for Fig. 14. The calculation is explicitly of

$$(\mathrm{Re}\ J/A)_{\mathrm{iso}} = (J_{V_V}/A)_{\mathrm{proton}} - (J_{V_V}/A)_{\mathrm{neutron}} + J_{\Delta_c},\tag{45}$$

using Eq. (42) and the integral of the Coulomb correction term, J_{Delta_c}, which for the WP OMP has the analytical form

$$J_{\Delta_c} = -\tfrac{2}{5}\pi\hbar ceZ\big((\mathcal{R}_C)^2 - \big(1.20\times A^{\frac{1}{3}}\mathrm{fm}\big)^2\big),\tag{46}$$

and for the KD and MD potential the Coulomb correction integral calculation is similar to Eq. (42) because of its Woods-Saxon functional form. Figure 18 shows some agreement at the low energy (for $28<A<60$) but it is more disparate at the high energy. Likewise at $A<20$ there is sharp disagreement between the two applicable potentials (MD and WP) for these light nuclei. The fine features are telling also, the wildly oscillatory behavior of the MD and WP integrals are indicative of the size of the neutron excess (this is to be expected because

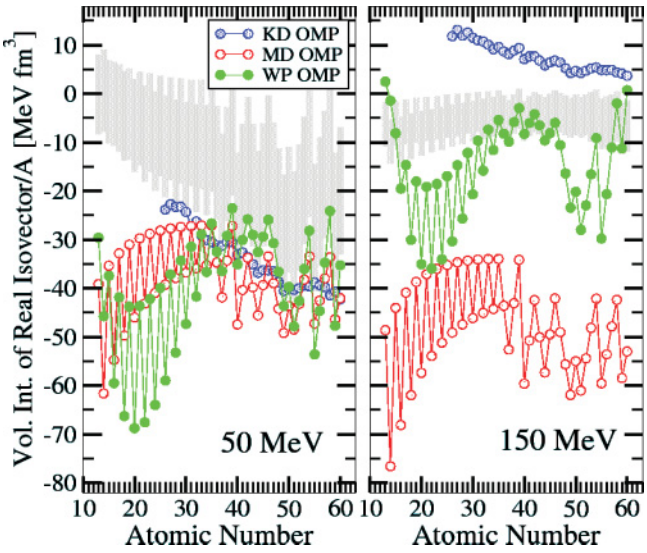

FIG. 18. (Color online) This is a calculation of the difference in the real component of the nuclear central potential integrals (volume and coulomb correction) between a proton and neutron projectile (about twice the actual isovector volume integral) for a representative selection of nuclei using three different global optical potentials. The nuclei were chosen to have nonzero $N - Z$ terms and to be close or on the line of stability. The nuclei are the same as used in Fig. 14. The dark blue semi-filled circular points are the calculation using the KD optical potential [1], the red unfilled circular points use the MD optical potential [2] and the light filled green circular data points are calculated using the WP potential of this work. The lines connecting the data points are there to make it easier for the eye to follow. The left panel used a 50 MeV nucleon projectile and the right panel uses a 150 MeV projectile where the differences in the three calculations become more pronounced. The light gray shaded area is the range of values for microscopic potentials which are described in the text in Sec. IV C.

they are similar to Gamow-Teller and Fermi sum rules which are proportional to $N - Z$ [143]), in the KD integrals this behavior has been quenched because the neutron and proton potentials lack the requisite similarity.

Figure 18 also has a light gray shaded area depicting a range of microscopic optical potentials isovector volume integrals. These microscopic potentials have been described in Sec. IV C and their isoscalar volume integrals depicted in Fig. 14. Overall the microscopic optical potentials have a systematically lower strength than the three OMPs, although it is encouraging to see that at the lower 50 MeV projectile energy there is a general agreement between all the potentials for target nucleons with $A > 28$. Some features of the microscopic potential isovector character are that it has a much smaller width at higher energies because the impulse approximation, where a free density-independent t-matrix is closer to being realized. Likewise the microscopic potential also shows an oscillatory $N - Z$ behavior in the isovector volume strength, for example the isovector character of ^{14}C is almost twice as big as ^{13}C because it has twice the neutron excess. At high energies the KD and WP isovector elements shrink and mimic the microscopic result better than the MD OMP which grows; this is deceiving, for the source of the magnitude shifts are not substantially isovector in origin but are almost entirely due to the Coulomb correction which is very much reduced in the WP and KD optical potentials at high energies but is energy independent in the MD optical potential.

The calculation of the explicit imaginary volume asymmetric potential is a distinct attribute of the WP optical potential described by this work. Calculating the isospin difference of the imaginary term for this potential is executed by

$$(\mathrm{Im}\ J/A)_{\mathrm{iso}} = (J_{W_V}/A + J_{W_S}/A)_{\mathrm{proton}} - (J_{W_V}/A + J_{W_S}/A)_{\mathrm{neutron}}, \quad (47)$$

where both the volume and surface terms are included as described by Eqs. (42)–(44). In contrast the KD OMP only has an implicit small imaginary asymmetric surface term by subtracting a neutron projectile reaction from a proton projectile reaction off the same target nucleus there is a significant imaginary difference coming from the disparity in isospin dependent volume strengths and Fermi energies. The MD potential has an imaginary isovector strength of zero. In Fig. 19 a plot of these imaginary volume integrals are depicted at a range between 50 MeV and 150 MeV projectile energies. The results are striking, this imaginary volume integral is quite large, often the same size or larger than the companion real piece. Having an imaginary asymmetry term, as the WP and KD optic potentials have, allows for a more nuanced optical potential which contains mechanisms

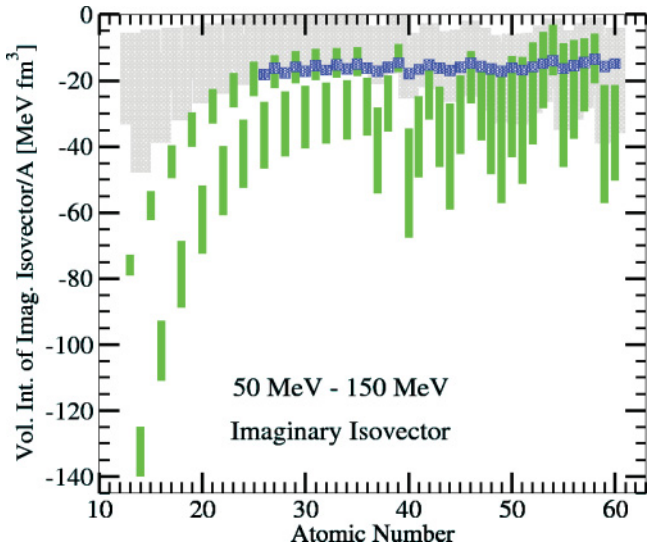

FIG. 19. (Color online) This is a calculation of the difference in the imaginary component of the central volume integrals between a proton and neutron projectile (about twice the isovector strength) for a representative selection of nuclei using the WP and KD global optical potential. The nuclei were chosen to have nonzero $N - Z$ terms and to be close or on the line of stability, the specific nuclei are listed in Fig. 14. The light green fill represents the range possible for nucleon projectile energies between 50 MeV and 150 MeV for the WP global optical potential of this work. The KD global optical potential (dark blue fill) is smaller and has a diminished range but its values are comparable to its real counterpart. The light gray shaded area is the range of values for microscopic potentials which are described in the text in Sec. IV C.

for charge-exchange resonances [143], important at these energies. Again, for further comparison, the microscopic optical potential range for the imaginary isovector element is depicted in light gray. It is systematically lower than the phenomenological optical potentials but is also is often much stronger than its real counterpart, especially at higher energies. The microscopic potential integral still carries large remnants of the $N - Z$ character in the results as does the WP OMP. The KD OMP is greatly reduced reminiscent of the real isovector volume element of Fig. 18. Incidentally, if a realistic imaginary Coulomb correction is added it would give a small positive volume element differential to the results depicted in Fig. 19 thus leading to better agreement between the phenomenological and microscopic potentials for this term.

A comparison of these asymmetric isovector volume integrals differences can me made to experiment. It is well understood that the asymmetry volume integral is tied to Gamow-Teller transitions in charge-exchange reactions which dominate at high energies [143]. The volume integral equations of Eqs. (42)–(47) are equivalent to doing a Fourier transform to momentum transfer (q) space set to zero. In this forward scattering case the inelastic aspect of the asymmetry terms dominates. This is because in the Coulomb distorted wave basis the long range Coulomb potential, which dictates extremely forward angle proton scattering, is external to the optical potential so the magnitude of the elastic scattering component is zero, likewise the neutron scattering elastic forward amplitude is zero. This extreme scattering has been recognized as being important in determining Gamow-Teller strengths [144,145]. If the difference is taken between the energy needed to initiate a proton-neutron charge-exchange and a neutron-proton charge-exchange for the same target nucleus (the difference in Q values derived from the mass excess values for the resultant final nuclei) this can be compared to the difference in the volume integrals which give the minimum energy, zero momentum transfer, nuclear density difference.

The volume integral for the Coulomb potential is infinite but it can easily be defined within the traditional nuclear radius, using the short range expression, used by all three OMPs under examination, which states that when $r < \mathcal{R}_C$:

$$J_C/A = \frac{4\pi}{A}\int_0^{\mathcal{R}_V A^{\frac{1}{3}}} f_{\text{coul}}(r, \mathcal{R}_C, A, N, Z) r^2 dr. \quad (48)$$

In the short range the Coulomb potential interferes with the nuclear force and contributes to the overall strength of the asymmetric volume element. The KD and MD optical potentials also include a separate Coulomb correction term while the potential of this work (WP) does not contain a separate Coulomb correction term but is part of the original short-range Coulomb term as detailed in Sec. V. These nuclear corrections are significant in the short range and must be included when illustrating short range differences between neutron and proton scattering.

To calculate the difference per nucleon in potential energy density at zero momentum transfer in the short range five terms are calculated

$$J_{\text{iso}} = (\text{Re } J/A + J_{\text{coul.corr.}}/A)_{\text{iso}} + (\text{Im } J/A)_{\text{iso}} + J_C/A - \Delta J_{\text{sr}}, \quad (49)$$

where the first line is the real nuclear potential energy density difference with the Coulomb correction included (Fig. 18). The second line is the imaginary nuclear potential energy density difference (Fig. 19). The last line is the short range Coulomb potential volume [Eq. (48)], up to the nuclear radius $\mathcal{R}_V$, and a zero point correction, ΔJ_{sr}. This correction is needed because of the weakened short ranged Coulomb volume that is used by all three potentials as dictated by Eq. (4). Since the Coulomb distorted wave basis sets zero nuclear scattering as defined by the traditional long range Coulomb form [Eq. (3)] and the short range volume element form actually used is 20% weaker then the traditional Coulomb potential, the true zero-scattering point has been shifted in the distorted wave Coulomb basis of neutron and proton scattering within the short range and this modification has to be normalized accordingly. Thus the correction is

$$\Delta J_{\text{sr}} = (0.2)\frac{4\pi}{A}\int_0^{\mathcal{R}_C A^{\frac{1}{3}}} \frac{Ze^2}{r} r^2 dr, \quad (50)$$

which is applied to all the potentials consistently.

In Figs. 20 and 21 there are depicted Q value (mass excess) differences for charge-exchange reactions ($Q(n,p) - Q(p,n)$) in black along with normalized volume integrals for the MD, WP, KD, and a typical microscopic $t - \rho$ optical potentials [122] for the 48 different sample target nuclei at a projectile energy of 150 MeV. The normalized optical potentials were calculated by using Eq. (49) and then multiplying that result by a constant density. The functional form results of the optical potential volume integrals are in remarkable agreement with the experimental Q value differences. Three of the four optical potentials mimic the shape and structure of the experimental mass excesses, following the global minimum at ^{13}C, local maxima and minima at ^{39}K and ^{40}K (dictated by factors of $N - Z$), and the general trends as nucleon number increases. A natural consequence of fitting elastic scattering data with a proton and neutron inclusive optical potential is the ability to mimic the Q values of the charge-exchange reactions at high energies given a simplistic constant density normalization factor even without these data being used as fitting constraints. This structure is remarkably also built into the microscopic optical potential which is a sum of the two-body nucleon-nucleon potentials [122]. The only optical potential that does poorly is the KD potential which was developed using separate potentials for proton and neutron scattering. The general conclusion is that by simultaneously fitting neutron and proton projectiles (or neutron-proton and proton-proton phase shifts in the case of the microscopic potentials) one automatically develops a potential which has the correct target dependant relative moduli strengths for the forward scattering volume integrals at high energy which are tied directly to both the mass difference and Gamow-Teller matrix elements.

The general systemic target shape is correct in Figs. 20, 21 for the MD, WP, and $t - \rho$ potentials but the magnitude

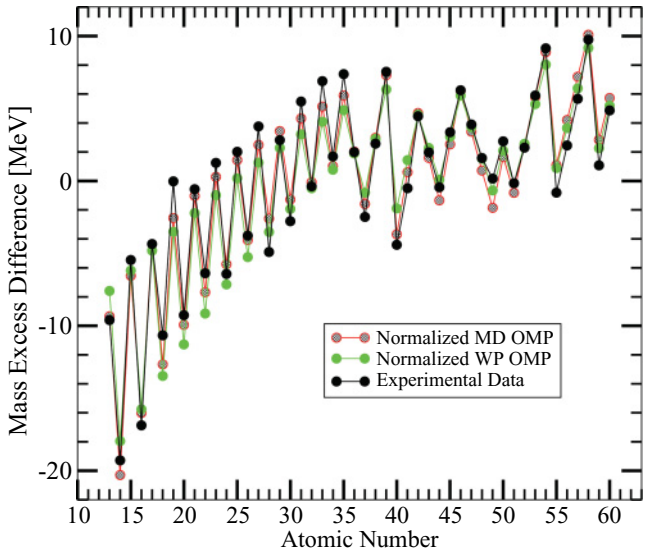

FIG. 20. (Color online) This plot depicts the total normalized energy difference ($J_{\rm iso}\rho_{\rm nuc}$) for the proton and neutron projectiles on a representative selection of nuclei using two different global optical potentials using potentials at projectile energy of 150 MeV. The nuclei were chosen to have nonzero $N-Z$ terms and to be close or on the line of stability, the specific nuclei are listed in Fig. 14. These calculations are compared to the difference in experimental mass excess energies for the charge-exchange reactions, $Q(n,p)-Q(p,n)$ from the same targets, the experimental data (dark black circles) are from Ref. [146]. The MD calculations, the unfilled red circles, have multiplied the results of Eq. (49) by .38 fm^{-3}, the WP calculations, the light filled green circles, has been multiplied by .16 fm^{-3}. The experimental mass excess energies shown here were not used to constrain the OMPs during the fitting procedure. Two other potential calculations along with experiment are shown in Fig. 21.

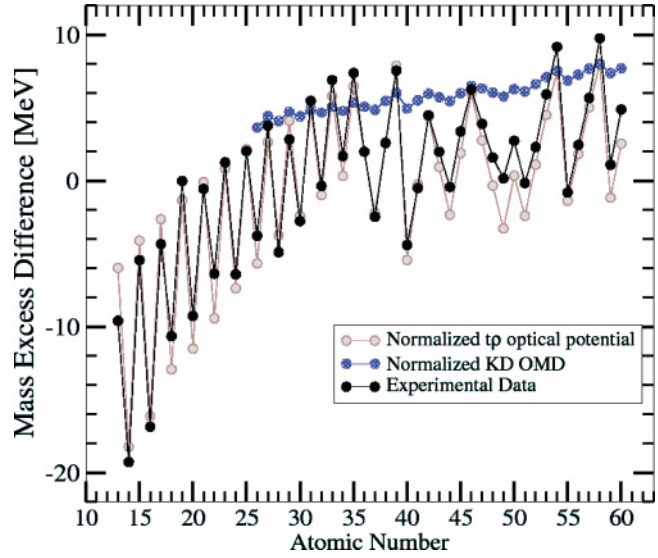

FIG. 21. (Color online) This plot depicts the total normalized energy difference ($J_{\rm iso}\rho_{\rm nuc}$) for the proton and neutron projectiles on a representative selection of nuclei using two different global optical potentials using potentials at projectile energy of 150 MeV. The nuclei were chosen to have nonzero $N-Z$ terms and to be close or on the line of stability, the specific nuclei are listed in Fig. 14. These calculations are compared to the difference in experimental mass excess energies for the charge-exchange reactions, $Q(n,p)-Q(p,n)$ from the same targets, the experimental data (dark black circles) are from Ref. [146]. The KD calculations, the filled blue circles, have multiplied the results of Eq. (49) by .17 fm^{-3}, the lighter gray circles (following the technique described in Ref. [122]), has been multiplied by 1.14 fm^{-3}. The experimental mass excess energies shown here were not used to constrain the OMPs during the fitting procedure.

differences are substantial. The constant density factor is 1.14 fm^{-3} for the microscopic potential, 0.38 fm^{-3} for the MD calculation (the isovector volume strength is three times the size of the microscopic calculation) and the WP OMP has 0.16 fm^{-3} for the constant density (the isovector volume strength is seven times the size of the microscopic). Additionally the MD optical potential has all its strength in the real component where the WP and microscopic potentials have isovector character distributed in both the real and imaginary term. Others have used charge-exchange differential cross sections to constrain the nucleon-nucleus optical potential asymmetric isovector term. Future work on this OMP could take that direction following the procedures as outlined in Refs. [134,147] which would help constrain these isovector magnitudes further.

The ramifications of the large asymmetric potential differences can be ascertained also with reactions that the global optical potentials are currently fitted to. Table IV examines the differences between the ^{40}Ar$(n,*)$ and ^{40}Ca$(n,*)$ cross sections with a 50 MeV and 150 MeV neutron projectile (calcium subtracted from argon). The large differences generated in the elastic and inelastic cross section predictions are highly dependent on the contrasts in the antisymmetric isovector term between the three potentials. This reaction was chosen because both $A=40$ nuclei are stable and there are dramatic differences between the potentials at $A=40$ in the asymmetric term. Using neutrons as projectiles also allows an ignorance

TABLE IV. This is a comparison of the strength of the asymmetry term at $A=40$. The calculation is the difference between neutron-nucleus total cross section calculations from scattering off of ^{40}Ar and ^{40}Ca at 50 MeV and 150 MeV projectile energies ($\sigma_{\rm Ar}-\sigma_{\rm Ca}$). The differences between the three optical potentials at high energies are mostly due to the isovector asymmetric term and pronounced and easily separable. At lower energies the differences fall within experimental deviation.

Energy MeV	Model	ΔReJ MeV fm^3	ΔImJ MeV fm^3	$\Delta\sigma_{\rm elast}$ mb	$\Delta\sigma_{\rm react}$ mb	$\Delta\sigma_{\rm tot}$ mb
	KD	+1.8	+0.4	+14	−28	−14
50	MD	+14.5	0.0	−36	−9	−45
MeV	WP	−10.8	+8.2	+68	−51	+17
	$t-\rho$	+14.0	+7.5	−18	−22	−40
	KD	+2.6	+0.5	−19	−4	−23
150	MD	+18.2	0.0	−106	−5	−111
MeV	WP	+3.1	+16.8	+188	−287	−99
	$t-\rho$	+2.1	+5.8	−6	−15	−21

of Coulomb effects and Coulomb correction terms. At the 50 MeV projectile energy the isovector differences are large however the calculations fall within one or two standards deviation of experimental error [93,148]. At the higher projectile energy of 150 MeV, where it can be assumed that the born and impulse approximations have validity, the effects of correlations, coupled channels and potential distortions are at a minimum. The extreme dramatic reduction in the inelastic cross section and increase in the elastic cross section predicted by the WP OMP differs wildly with the predicted large decrease in the elastic cross section seen by the MD potential. Likewise the KD and microscopic potentials offers a third very realistic conclusion; that the differences between ^{40}Ar(n,*) and ^{40}Ca(n,*) cross sections with a 150 MeV neutron projectile are relatively minor. There is at present no high energy ^{40}Ar(n,*) data to confer which optical potential is closest to experiment. Experiments calculating the ^{40}Ar cross sections would be a welcome addition as well as would other high energy neutron reaction data like recent experiments detailed in Refs. [46,103] which, if use $N \neq Z$ target nuclei, are sensitive to the isovector term.

VI. CONCLUSION

The motivations for this work were to construct a phenomenological nucleon-nucleus global optical potential that is suited for a wide range of nuclei targets and projectile energies which are within capacity of the exotic beam accelerators presently running and under development. We have succeeded in creating one isospin dependent potential which fits target nuclei $12 \leqslant A \leqslant 60$ and a projectile energy of 30 MeV $\leqslant E \leqslant 160$ MeV. It compares well with two other recent global optical potentials [1,2], its advantages are that it is one continuous optical potential which is designed to do systematic studies on mirror nuclei and chains of isotopes (a observable calculator has also been made available to researchers to quickly use this potential for their own research [11]). We have also included an imaginary asymmetry term which is missing from other recent global optical potentials and have given comparative analysis on how the asymmetric potential terms in the three potentials dramatically differ from each other, microscopic potentials and the ramifications to experimentally testable observables. It was also ascertained that a benefit of fitting the proton and neutron observables simultaneously is the ability to accurately define the structure of the mass excesses for the charge-exchange reactions.

There also was a critical examination of the validity of the traditional linear proportionality of $N - Z$ applied in the asymmetry term. An examination of the calculation of the calcium and chromium experimental observables produced at 65 MeV projectile energy show a continuing failure to produce great fits along the isotopic chain, indicative of a breakdown of this linear asymmetry ansatz. Further low and high energy experimental studies of chains of isotopes would help guide future theoretical studies of the asymmetry term.

Future work could extend this potential to heavier targets, test other forms of asymmetry potentials, examine spin-spin terms, use charge-exchange information to constrain data, and determine algorithms to better weight the scattering observables. To better constrain the terms more elastic scattering data from traditional and exotic nuclei data are needed especially at the higher energies.

ACKNOWLEDGMENTS

S.P.W. gratefully acknowledges the hospitality of the Physics Department at The Florida State University, especially Kirby Kemper, during the author's sabbatical leave where this work was begun. We are also indebted to a TeraGrid grant (PHY060025N), funded by the National Science Foundation, in which a bulk of the computational research was done. This work was also graciously supported by Eckerd College internal grants which allowed students to work on this project over ensuing summers including a special debt to Nicholas Crotty for retrieving the experimental data and to Eva Romero Luna for her help in arranging the final figures.

[1] A. J. Koning and J. P. Delaroche, Nucl. Phys. **A713**, 231 (2003).
[2] D. G. Madland, in Proceedings of OECD/NEA Specialists Meeting on Nucleon-Nucleus Optical Model to 200 MeV (1997), p. 129, this can also be found at arXiv:nucl-th/9702035v1.
[3] F. D. Becchetti and G. W. Greenlees, Phys. Rev. **182**, 1190 (1969).
[4] J. P. Jeukenne, A. Lejeune, and C. Mahaux, Phys. Rev. C **16**, 80 (1977), and references therein.
[5] A. Nadasen, P. Schwandt, P. P. Singh, W. W. Jacobs, A. D. Bacher, P. T. Debevec, M. D. Kaitchuck, and J. T. Meek, Phys. Rev. C **23**, 1023 (1981).
[6] R. L. Varner, W. J. Thompson, T. L. McAbee, E. J. Ludwig, and T. B. Clegg, Phys. Rep. **201**, 57 (1991).
[7] J. Rapaport, V. Kulkarni, and R. W. Finlay, Nucl. Phys. **A330**, 15 (1997).
[8] E. Bauge, J. P. Delaroche, and M. Girod, Phys. Rev. C **58**, 1118 (1998).
[9] B. Morillon and P. Romain, Phys. Rev. C **76**, 044601 (2007).
[10] X. Li and C. Cai, Nucl. Phys. **A801**, 43 (2008).
[11] S. P. Weppner, G. W. Diffendale, and G. Vittorini, Optical potential calculator, World Wide Web electronic publication (2008), http://home.eckerd.edu/∼weppnesp/optical.
[12] M. A. Melkanoff, T. Sawada, and J. Raynal, *Methods in Computational Physics* (Academic Press, New York, 1966), Vol. VI.
[13] A. J. Koning, S. Hilaire, and M. C. Duijvestijn, in *Proceedings of the International Conference on Nuclear Data for Science and Technology* (AIP, New York, 2004), Vol. 769, pp. 1154–1159.
[14] A. J. Koning, S. Hilaire, and M. C. Duijvestijn, TALYS: Comprehensive nuclear reaction modeling, World Wide Web electronic publication (2008), http://www.talys.eu.
[15] J. Raynal, Phys. Rev. C **71**, 057602 (2005), and references therein.

[16] A. R. Barnett, Comput. Phys. Commun. **27**, 147 (1982).
[17] W. Press, B. Flannery, S. Teukolsky, and W. Vetterling, *Numerical Recipes in FORTRAN: The Art of Scientific Computing*, 2nd ed. (Cambridge University Press, Cambridge, UK, 1992), Chap. 10.
[18] P. Bratley and B. Fox, ACM Transactions on Mathematical Software **14**, 88 (1988).
[19] A. A. Korsheninnikov, E. Y. Nikolskii, T. Kobayashi, D. V. Aleksandrov, M. Fujimaki, H. Kumagai, A. A. Ogloblin, A. Ozawa, I. Tanihata, Y. Watanabe *et al.*, Phys. Lett. **B343**, 53 (1995).
[20] M. Ieiri, H. Sakaguchi, M. Nakamura, H. Sakamoto, H. Ogawa, M. Yosoi, T. Ichihara, N. Isshiki, Y. Takeuchi, H. Togawa *et al.*, Nucl. Instrum. Methods Phys. Res. A **257**, 253 (1987).
[21] P. D. Greaves, V. Hnizdo, J. Lowe, and O. Karban, Nucl. Phys. **A179**, 1 (1972).
[22] E. Fabrici, S. Micheletti, M. Pignanelli, F. G. Resmini, R. De Leo, G. D'Erasmo, and A. Pantaleo, Phys. Rev. C **21**, 844 (1980).
[23] A. A. Rush, E. J. Burge, and D. A. Smith, Nucl. Phys. **A166**, 378 (1971).
[24] J. J. Menet, E. E. Gross, J. J. Malanify, and A. Zucker, Phys. Rev. C **4**, 1114 (1971).
[25] H. Ohnuma, B. A. Brown, D. Dehnhard, K. Furukawa, T. Hasegawa, S. Hayakawa, N. Hoshino, K. Ieki, M. Kabasawa, K. Maeda *et al.*, Nucl. Phys. **A456**, 61 (1986).
[26] N. M. Clarke, E. J. Burge, and D. A. Smith, Nucl. Phys. **A157**, 145 (1970).
[27] R. F. Carlson, A. J. Cox, T. N. Nasr, M. S. D. Jong, D. L. Ginther, D. K. Hasell, A. M. Sourkes, W. T. H. van Oers, and D. J. Margaziotis, Nucl. Phys. **A445**, 57 (1985).
[28] M. Pignanelli, S. Micheletti, R. De Leo, S. Brandenburg, and M. N. Harakeh, Phys. Rev. C **33**, 40 (1986).
[29] L. N. Blumberg, E. E. Gross, A. V. der Woude, A. Zucker, and R. H. Bassel, Phys. Rev. **147**, 812 (1966).
[30] B. V. Przewoski, P. D. Eversheim, F. Hinterberger, U. Lahr, J. Campbell, J. Gtz, M. Hammans, R. Henneck, G. Masson *et al.*, Nucl. Phys. **A528**, 159 (1991).
[31] V. M. Hannen, K. Amos, A. M. van den Berg, R. K. Bieber, P. K. Deb, F. Ellinghaus, D. Frekers, M. Hagemann, M. N. Harakeh, J. Heyse *et al.*, Phys. Rev. C **67**, 054321 (2003).
[32] J. R. Comfort, S. M. Austin, P. T. Debevec, G. L. Moake, R. W. Finlay, and W. G. Love, Phys. Rev. C **21**, 2147 (1980).
[33] A. E. Taylor and E. Wood, Nucl. Phys. **25**, 642 (1961).
[34] V. I. Grancev, V. I. Konfederatenko, V. A. Kornilov, O. F. Nemec, R. G. Rudenko, M. V. Sokolov, and B. G. Struzhko, Ukr. J. Phys. **28**, 506 (1983).
[35] J. A. Fannon, E. J. Burge, D. A. Smith, and N. K. Ganguly, Nucl. Phys. **A97**, 263 (1967).
[36] S. F. Collins, G. G. Shute, B. M. Spicer, V. C. Officer, I. Morrison, K. A. A. D. W. Devins, D. L. Friesel, and W. P. Jones, Nucl. Phys. **A380**, 445 (1982).
[37] E. Colombo, R. D. Leo, J. L. Escudie, E. Fabrici, S. Micheletti, M. Pignanelli, and F. Resmini, J. Phys. Soc. Jpn. Suppl. **44**, 543 (1978).
[38] C. B. Fulmer, J. B. Ball, A. Scott, and M. L. Whitten, Phys. Rev. **181**, 1565 (1969).
[39] S. Kato, K. Okada, M. Kondo, K. Hosono, T. Saito, N. Matsuoka, K. Hatanaka, T. Noro, S. Nagamachi, H. Shimizu *et al.*, Phys. Rev. C **31**, 1616 (1985).
[40] H. Ohnuma, N. Hoshino, K. Ieki, M. Iwase, H. Shimizu, H. Toyokawa, T. Hasegawa, K. Nisimura, M. Yasue, H. Kabasawa *et al.*, Nucl. Phys. **A514**, 273 (1990).
[41] E. Fabrici, S. Micheletti, M. Pignanelli, F. G. Resmini, R. De Leo, G. D'Erasmo, A. Pantaleo, J. L. Escudié, and A. Tarrats, Phys. Rev. C **21**, 830 (1980).
[42] A. Ingemarsson, J. Nyberg, P. U. Renberg, O. Sundberg, R. F. Carlson, A. Auce, R. Johansson, G. Tibell, B. C. Clark, L. K. Kerr *et al.*, Nucl. Phys. **A653**, 341 (1999).
[43] C. Rolland, B. Geoffrion, N. Marty, M. Morlet, B. Tatischeff, and A. Willis, Nucl. Phys. **80**, 625 (1966).
[44] R. F. Carlson, A. J. Cox, J. R. Nimmo, N. E. Davison, S. A. Elbakr, J. L. Horton, A. Houdayer, A. M. Sourkes, W. T. H. van Oers, and D. J. Margaziotis, Phys. Rev. C **12**, 1167 (1975).
[45] G. M. Lerner and J. B. Marion, Nucl. Phys. **A193**, 593 (1972).
[46] A. Auce, A. Ingemarsson, R. Johansson, M. Lantz, G. Tibell, R. F. Carlson, M. J. Shachno, A. A. Cowley, G. C. Hillhouse, N. M. Jacobs *et al.*, Phys. Rev. C **71**, 064606 (2005).
[47] K. Strauch and F. Titus, Phys. Rev. **103**, 200 (1956).
[48] J. M. Cameron, J. R. Richardson, W. T. H. van Oers, and J. W. Verba, Phys. Rev. **167**, 908 (1968).
[49] H. O. Meyer, P. Schwandt, W. W. Jacobs, and J. R. Hall, Phys. Rev. C **27**, 459 (1983).
[50] E. Khan, Y. Blumenfeld, N. V. Giai, T. Suomijarvi, N. Alamanos, F. Auger, G. Colo, N. Frascaria, A. Gillibert, T. Glasmacher *et al.*, Phys. Lett. **B490**, 45 (2000).
[51] W. Bauhoff, S. F. Collins, R. S. Henderson, G. G. Shute, B. M. Spicer, V. C. Officer, K. A. Amos, I. Morrison, D. W. Devins, D. L. Friesel *et al.*, Nucl. Phys. **A410**, 180 (1983).
[52] H. Sakaguchi, M. Nakamura, K. Hatanaka, A. Goto, T. Noro, F. Ohtani, H. Sakamoto, H. Ogawa, and S. Kobayashi, Phys. Rev. C **26**, 944 (1982).
[53] J. K. Jewell, L. A. Riley, P. D. Cottle, K. W. Kemper, T. Glasmacher, R. W. Ibbotson, H. Scheit, M. Chromik, Y. Blumenfeld, S. E. Hirzebruch *et al.*, Phys. Lett. **B454**, 181 (1999).
[54] A. E. Taylor and E. Wood, Nucl. Phys. **25**, 642 (1961).
[55] J. M. Emmerson, J. C. W. Madden, C. M. P. Johnson, N. Middlemas, A. B. Clegg, and W. S. C. Williams, Nucl. Phys. **77**, 305 (1966).
[56] J. J. Kelly, W. Bertozzi, T. N. Buti, J. M. Finn, F. W. Hersman, C. Hyde-Wright, M. V. Hynes, M. A. Kovash, B. Murdock, B. E. Norum *et al.*, Phys. Rev. C **39**, 1222 (1989).
[57] E. Becheva, Y. Blumenfeld, E. Khan, D. Beaumel, J. M. Daugas, F. Delaunay, C. E. Demonchy, A. Drouart, M. Fallot, A. Gillibert *et al.*, Phys. Rev. Lett. **96**, 012501 (2006).
[58] V. Comparat, R. Frascaria, N. Marty, M. Morlet, and A. Willis, Nucl. Phys. **A221**, 403 (1974).
[59] D. K. Hasell, N. E. Davison, T. N. Nasr, B. T. Murdoch, A. M. Sourkes, and W. T. H. van Oers, Phys. Rev. C **27**, 482 (1983).
[60] A. A. Rush, E. J. Burge, V. E. Lewis, D. A. Smith, and N. K. Ganguly, Nucl. Phys. **A104**, 340 (1967).
[61] H. Ohnuma, J. Kasagi, F. Kakimoto, S. Kubono, and K. Koyama, J. Phys. Soc. Jpn. **48**, 1812 (1980).
[62] N. Alamanos, A. Pakou, A. Lagoyannis, and A. Musumarra, Nucl. Phys. **A660**, 406 (1999).
[63] K. Hatanaka, M. Fujiwara, K. Hosono, N. Matsuoka, T. Saito, and H. Sakai, Phys. Rev. C **29**, 13 (1984).
[64] P. Schwandt, H. O. Meyer, W. W. Jacobs, A. D. Bacher, S. E. Vigdor, M. D. Kaitchuck, and T. R. Donoghue, Phys. Rev. C **26**, 55 (1982).

[65] P. D. Cottle, Z. Hu, B. V. Pritychenko, J. A. Church, M. Fauerbach, T. Glasmacher, R. W. Ibbotson, K. W. Kemper, L. A. Riley, H. Scheit *et al.*, Phys. Rev. Lett. **88**, 172502 (2002).
[66] E. Khan, T. Suomijarvi, Y. Blumenfeld, V. G. Nguyen, N. Alamanos, F. Auger, E. Bauge, D. Beaumel, J. P. Delaroche, P. Delbourgo-Salvador *et al.*, Nucl. Phys. **A694**, 103 (2001).
[67] R. Alarcon, J. Rapaport, R. T. Kouzes, W. H. Moore, and B. A. Brown, Phys. Rev. C **31**, 697 (1985).
[68] H. Scheit, F. Maréchal, T. Glasmacher, E. Bauge, Y. Blumenfeld, J. P. Delaroche, M. Girod, R. W. Ibbotson, K. W. Kemper, J. Libert *et al.*, Phys. Rev. C **63**, 014604 (2000).
[69] N. T. Okumusoglu, J. Birchall, M. S. A. L. Al-Ghazi, C. Lapointe, J. S. C. Mckee, H. E. Conzett, R. M. Larimer, and P. Von-Rossen, Nucl. Phys. **A393**, 45 (1983).
[70] R. H. McCamis, T. N. Nasr, J. Birchall, N. E. Davison, W. T. H. van Oers, P. J. T. Verheijen, R. F. Carlson, A. J. Cox, B. C. Clark, E. D. Cooper *et al.*, Phys. Rev. C **33**, 1624 (1986).
[71] R. F. Carlson, A. J. Cox, N. E. Davison, T. Eliyakut-Roshko, R. H. McCamis, and W. T. H. van Oers, Phys. Rev. C **49**, 3090 (1994).
[72] G. S. Mani, D. T. Jones, and D. Jacques, Nucl. Phys. **A165**, 384 (1971).
[73] T. Noro, H. Sakagochi, M. Nakamura, K. Natanaka, F. Ohtani, H. Sakamoto, and S. Kobayashi, Nucl. Phys. **A366**, 189 (1989).
[74] S. Sakaguchi, *Memoirs of the Faculty of Science, Kyoto University, Science of Physics, Astrophysics, Geophysics and Chemistry*, *36*, No. 2 (1993) Article 4.
[75] L. W. Woo, N. S. Wall, P. G. Roos, P. H. Debenham, K. Kwiatkowski, and A. Nadasen, Phys. Rev. C **29**, 794 (1984).
[76] T. N. Nasr, A. M. Sourkes, D. J. Margaziotis, R. L. Carlson, and A. J. Cox, Can. J. Phys. **56**, 56 (1978).
[77] R. F. Carlson, At. Data Nucl. Data Tables **63**, 93 (1996).
[78] F. E. Bertrand and R. W. Peelle, Phys. Rev. C **8**, 1045 (1973).
[79] R. De Leo, H. Akimune, N. Blasi, I. Daito, Y. Fujita, M. Fujiwara, S. I. Hayakawa, S. Hatori, K. Hosono, H. Ikegami *et al.*, Phys. Rev. C **53**, 2718 (1996).
[80] R. H. McCamis, N. E. Davison, W. T. H. van Oers, R. F. Carlson, and A. J. Cox, Can. J. Phys. **64**, 685 (1986).
[81] M. P. Fricke, E. E. Gross, and A. Zucker, Phys. Rev. **163**, 1153 (1967).
[82] B. W. Ridley and J. F. Turner, Nucl. Phys. **58**, 497 (1964).
[83] M. P. Fricke, E. E. Gross, B. J. Morton, and A. Zucker, Phys. Rev. **156**, 1207 (1967).
[84] H. Sakaguchi, M. Nakamura, K. Hatanaka, T. Noro, F. Ohtani, H. Sakamoto, H. Ogawa, and S. Kobayashi, Phys. Lett. **B99**, 92 (1981).
[85] P. Dimbylow, Physics in Medicine and Biology **25**, 637 (1980).
[86] T. Niizeki, H. Orihara, K. Ishii, K. Maeda, M. Kabasawa, Y. Takahashi, and K. Miura, Nucl. Instrum. Methods Phys. Res. A **287**, 455 (1990).
[87] M. Ibaraki, M. Baba, Tak. Miura, Y. Nauchi, Y. Hirasawa, N. Hirakawa, H. Nakashima, S. Meigo, O. Iwamoto, Su. Tanaka, J. Nucl. Sci. Technol. Suppl. **1**, 683 (2000).
[88] J. H. Osborne, F. P. Brady, J. L. Romero, J. L. Ullmann, D. S. Sorenson, A. Ling, N. S. P. King, R. C. Haight, J. Rapaport, R. W. Finlay *et al.*, Phys. Rev. C **70**, 054613 (2004).
[89] K. Amos and S. Karataglidis, Phys. Rev. C **65**, 057603 (2002).
[90] J. Klug, J. Blomgren, A. Ataç, B. Bergenwall, A. Hildebrand, C. Johansson, P. Mermod, L. Nilsson, S. Pomp, U. Tippawan *et al.*, Phys. Rev. C **68**, 064605 (2003).
[91] P. K. Deb, K. Amos, S. Karataglidis, M. B. Chadwick, and D. G. Madland, Phys. Rev. Lett. **86**, 3248 (2001).
[92] R. W. Finlay, W. P. Abfalterer, G. Fink, E. Montei, T. Adami, P. W. Lisowski, G. L. Morgan, and R. C. Haight, Phys. Rev. C **47**, 237 (1993).
[93] W. P. Abfalterer, F. B. Bateman, F. S. Dietrich, R. W. Finlay, R. C. Haight, and G. L. Morgan, Phys. Rev. C **63**, 044608 (2001).
[94] National Nuclear Data Center, World Wide Web electronic publication (2008), http://www.nndc.bnl.gov.
[95] K. Amos, S. Karataglidis, and P. K. Deb, Phys. Rev. C **65**, 064618 (2002).
[96] P. K. Deb and K. Amos, Phys. Rev. C **69**, 064608 (2004).
[97] R. P. DeVito, S. M. Austin, U. E. P. Berg, R. DeLeo, and W. A. Sterrenburg, Phys. Rev. C **28**, 2530 (1983).
[98] E. L. Hjort, F. P. Brady, J. R. Drummond, B. McEachern, J. H. Osborne, J. L. Romero, D. S. Sorenson, and H. H. K. Tang, Phys. Rev. C **53**, 237 (1996).
[99] R. P. DeVito, S. M. Austin, W. Sterrenburg, and U. E. P. Berg, Phys. Rev. Lett. **47**, 628 (1981).
[100] E. L. Hjort, F. P. Brady, J. L. Romero, J. R. Drummond, D. S. Sorenson, J. H. Osborne, B. McEachern, and L. F. Hansen, Phys. Rev. C **50**, 275 (1994).
[101] R. J. Charity, J. M. Mueller, L. G. Sobotka, and W. H. Dickhoff, Phys. Rev. C **76**, 044314 (2007).
[102] A. Öhrn, J. Blomgren, P. Andersson, A. Ataç, C. Gustavsson, J. Klug, P. Mermod, S. Pomp, P. Wolniewicz, M. Österlund *et al.*, Phys. Rev. C **77**, 024605 (2008).
[103] B. Abu-Ibrahim, W. Horiuchi, A. Kohama, and Y. Suzuki, Phys. Rev. C **77**, 034607 (2008).
[104] F. E. Bertrand and R. W. Peelle, Phys. Rev. C **8**, 1045 (1973).
[105] A. E. Taylor and E. Wood, Nucl. Phys. **25**, 642 (1961).
[106] C. Olmer, A. D. Bacher, G. T. Emery, W. P. Jones, D. W. Miller, H. Nann, P. Schwandt, S. Yen, T. E. Drake, and R. J. Sobie, Phys. Rev. C **29**, 361 (1984).
[107] H. S. Liers, R. N. Boyd, C. H. Poppe, J. A. Sievers, and D. L. Watson, Phys. Rev. C **2**, 1399 (1970).
[108] K. Kwiatkowski and N. S. Wall, Nucl. Phys. **A301**, 349 (1978).
[109] P. G. Roos and N. S. Wall, Phys. Rev. **140**, B1237 (1965).
[110] Y. Blumenfeld, E. Khan, F. Maréchal, and T. Suomijarvi, Pramana J. Phys. **57**, 493 (2001).
[111] S. G. Cooper, Nucl. Phys. **A618**, 87 (1997).
[112] G. H. Rawitscher and D. Lukaszek, Phys. Rev. C **69**, 044608 (2004).
[113] L. N. Blumberg, E. E. Gross, A. V. D. Woude, A. Zucker, and R. H. Bassel, Phys. Rev. **147**, 812 (1966).
[114] R. M. Craig, J. C. Dore, J. Lowe, and D. L. Watson, Nucl. Phys. **86**, 113 (1966).
[115] V. Hnizdo, O. Karban, J. Lowe, G. W. Greenlees, and W. Makofske, Phys. Rev. C **3**, 1560 (1971).
[116] G. W. Greenlees, V. Hnizdo, O. Karban, J. Lowe, and W. Makofske, Phys. Rev. C **2**, 1063 (1970).
[117] P. K. Deb and K. Amos, Phys. Rev. C **62**, 024605 (2000).
[118] N. C. Francis and K. M. Watson, Phys. Rev. **92**, 291 (1953).
[119] K. M. Watson, Phys. Rev. **89**, 575 (1953).
[120] K. Amos, P. J. Dortmans, H. V. Geramb, S. Karataglidis, and J. Raynal, in *Advances in Nuclear Physics*, Vol. 25, edited by J. W. Negele and E. Vogt (Plenum Publishers, New York, 2000), and references therein.

[121] C. R. Chinn, C. Elster, and R. M. Thaler, Phys. Rev. C **48**, 2956 (1993).
[122] C. R. Chinn, C. Elster, R. M. Thaler, and S. P. Weppner, Phys. Rev. C **52**, 1992 (1995).
[123] S. P. Weppner, C. Elster, and D. Hüber, Phys. Rev. C **57**, 1378 (1998).
[124] R. Machleidt, Phys. Rev. C **63**, 024001 (2001).
[125] R. B. Wiringa, V. G. J. Stoks, and R. Schiavilla, Phys. Rev. C **51**, 38 (1995).
[126] V. G. J. Stoks, R. A. M. Klomp, C. P. F. Terheggen, and J. J. de Swart, Phys. Rev. C **49**, 2950 (1994).
[127] C. J. Horowitz, D. P. Murdoch, and B. D. Serot, in *Computational Nuclear Physics 1*, edited by K. Langanke, J. A. Maruhn, and S. E. Koonin (Springer-Verlag, Berlin, 1991).
[128] J. J. Rusnak and R. J. Furnstahl, Nucl. Phys. **A627**, 495 (1997).
[129] A. M. Lane, Nucl. Phys. **35**, 676 (1962).
[130] G. R. Satchler, in *Isospin in Nuclear Physics*, edited by D. H. Wilkinson (North-Holland, New York, 1969), p. 389.
[131] G. R. Satchler, Nucl. Phys. **A91**, 75 (1967).
[132] A. Kerman, M. McManus, and R. M. Thaler, Ann. Phys. (NY) **8**, 551 (1959).
[133] R. Álvarez-Rodriguez, E. Moya de Guerra, and P. Sarriguren, Phys. Rev. C **71**, 044308 (2005).
[134] E. Bauge, J. P. Delaroche, and M. Girod, Phys. Rev. C **63**, 024607 (2001).
[135] J. D. Carlson, D. A. Lind, and C. D. Zafiratos, Phys. Rev. Lett. **30**, 99 (1973).
[136] C. Wong, S. M. Grimes, and R. W. Finlay, Phys. Rev. C **29**, 1710 (1984).
[137] J. P. Jeukenne, A. Lejeune, and C. Mahaux, Phys. Rev. C **15**, 10 (1977).
[138] J. Rapaport, Phys. Lett. **B92**, 233 (1980).
[139] H.-W. H. E. Epelbaum and U.-G. Meißner, arXiv:0811.338v1 [nucl-th] (2008) (to be published in Rev. Mod. Phys).
[140] G. A. Miller and W. T. H. van Oers, *Symmetries and Fundamental Interactions in Nuclei* (World Scientific, Singapore, 1995), pp. 127–166.
[141] Z. H. Li and U. Lombardo, Phys. Rev. C **78**, 047603 (2008).
[142] G. Audi and A. H. Wapstra, Nucl. Phys. **A595**, 409 (1995).
[143] F. Osterfeld, Rev. Mod. Phys. **64**, 491 (1992).
[144] C. D. Goodman, C. A. Goulding, M. B. Greenfield, J. Rapaport, D. E. Bainum, C. C. Foster, W. G. Love, and F. Petrovich, Phys. Rev. Lett. **44**, 1755 (1980).
[145] Y. Fujita, T. Adachi, P. von Brentano, G. P. A. Berg, C. Fransen, D. D. Frenne, H. Fujita, K. Fujita, K. Hatanaka, E. Jacobs *et al.*, Phys. Rev. Lett. **95**, 212501 (2005), and references therein.
[146] G. Audi, A. H. Wapstra, and C. Thibault, Nucl. Phys. **A729**, 337 (2006).
[147] A. M. Lane, Phys. Rev. Lett. **8**, 171 (1962).
[148] R. R. Winters, R. F. Carlton, C. H. Johnson, N. W. Hill, and M. R. Lacerna, Phys. Rev. C **43**, 492 (1991).